Solvation Ultrafast Dynamics of Reactions. 8. Acid−Base Reactions in Finite-Sized Clusters of Naphthol in Ammonia, Water, and Piperidine

S. K. Kim,[†] J. J. Breen,[‡] D. M. Willberg,[§] L. W. Peng,[⊥] A. Heikal, J. A. Syage,[∥] and A. H. Zewail*

Arthur Amos Noyes Chemical Physics Laboratory,[⊖] California Institute of Technology, Pasadena, California 91125

Received: August 26, 1994; In Final Form: November 11, 1994[⊗]

In this contribution, studies of the dynamics of proton-transfer reactions in solvent cages are presented, building on earlier work [Breen, J. J.; et al. *J. Chem. Phys.* **1990**, *92*, 805. Kim, S. K.; et al. *Chem. Phys. Lett.* **1994**, *228*, 369]. The acid−base system studied in a molecular beam is 1-naphthol as a solute and ammonia, piperidine, or water as the solvent, with the number of solvent molecules (n) varying. The rates and threshold for proton transfer have been found to be critically dependent on the number and type of solvent molecules: $n = 2$ for piperidine and $n = 3$ for ammonia; no proton transfer was observed for water up to $n = 21$. With subpicosecond time resolution, we observe a biexponential transient for the $n = 3$ cluster with ammonia. From these observations and the high accuracy of the fits, we provide the rate of the proton transfer at short times and the solvent reorganization at longer times. From studies of the effect of the total energy, the isotope substitution, and the number and type of solvent molecules, we discuss the nature of the transfer and the interplay between the local structure of the base solvent and the dynamics. The effective shape of the potential energy surface is discussed by considering the anharmonicity of the reactant states and the Coulombic interaction of ion-pair product states. Tunneling is related to the nature of the potential and to measurements specific to the isotope effect and energy dependence. Finally, we discuss a simple model for the reaction in finite-sized clusters, which takes into account the proton affinity and the dielectric shielding of the solvent introduced by the local structure.

I. Introduction

Proton transfer is ubiquitous in chemistry and biology (for some reviews, see refs 1−3). A key point in the measurements of proton-transfer rates is the ability to induce an acid−base reaction on a relatively short time scale ("pH jump") and to follow the change with time. Since the first report by Weber[4] in 1931 for the evidence of excited-state proton transfer, Förster[5] and Weller[6] showed that with light such instantaneous changes of the pK_a can be induced by excitation to the excited state. By using a four-level description, the Förster cycle, one can deduce the energetics as follows:

$$N_A[h\nu(A^*H \leftrightarrow AH) - h\nu(A^{*-} \leftrightarrow A^-)] = \Delta H_d(AH) - \Delta H_d(A^*H) \quad (1)$$

where AH is the acid and A^- is the conjugate base. The asterisk denotes the excited state, $h\nu$ represents the excitation energy between origins, N_A is the Avogadro number, and ΔH_d is the enthalpy of deprotonation. The enthalpy of deprotonation is related to the pK_a of the acid by the following thermodynamic relation when the change of entropy is neglected:

$$2.303RT[pK_a(AH) - pK_a(A^*H)] = \Delta H_d(AH) - \Delta H_d(A^*H) \quad (2)$$

That is, the enthalpy of deprotonation in the excited state decreases compared to that in the ground state with a significant increase in pK_a introduced by the excitation.

Fundamental to the proton-transfer reaction are the energetics of the initial and final states and the dynamical structure of the solvent. With femtosecond and picosecond time resolution, it is possible to study the elementary processes of structural changes due to solvent organization. Here, the system under study is 1-naphthol (referred to here as AH or 1-NpOH). The pK_a of 1-NpOH in solution is determined to be 9.4 in the ground state and 0.5 ± 0.2 in the excited state.[7] This large change in pK_a by the excitation makes it possible to induce the acid−base reaction on a very short time scale.

In solutions and in clusters, the naphthol systems have been studied to elucidate the proton-transfer mechanism. Spectroscopically, the broadening of the absorption peaks and the red shift of the emission have been used as indicators of proton transfer. Leutwyler's group[8,9] carried out thorough spectroscopic studies of 1-NpOH clusters with solvent molecules, such as water, ammonia, methanol, and piperidine, and deduced the energetics and the approximate size dependence for the onset of the process. In solutions, measurement of the rise time of the red-shifted emission can give the time constant for proton transfer, and many groups have been involved in such studies. For naphthols in water (and other solvents), the groups of Robinson and Clark[10] have studied the proton transfer in pure water and in mixed solvents; they reported 32 ps for pure water. Eigen's early studies[11] of acid solutions provided the dissociation and recombination rates (hence, equilibrium constants) and proposed a local structure for the proton, $(H_9O_4)^+$, in water. Robinson proposed, based on his studies, that in water the

[†] Arthur Amos Noyes Research Fellow.
[‡] Present address: Department of Chemistry, Indiana University−Purdue University, Indianapolis, IN 46205.
[§] Present address: Division of Engineering and Applied Science, California Institute of Technology, Pasadena, CA 91125.
[⊥] Present address: Sandia National Laboratories, Organization 8713, Livermore, CA 94551.
[∥] Permanent address: The Aerospace Corporation, Los Angeles, CA 90009.
[⊖] Contribution No. 8979.
[⊗] Abstract published in *Advance ACS Abstracts,* May 1, 1995.

0022-3654/95/2099-7421$09.00/0

hydration involves an instantaneous structure of 4 ± 1 water molecules, consistent with Eigen's suggestion. However, since the experiments were conducted in the bulk, there was no direct evidence of such structures. Kelley's group[12] has measured the proton-transfer rates for matrix-isolated naphthol–ammonia complexes. These studies gave 22 ps for the 1-NpOH·$(NH_3)_3$ complex in a matrix of argon. By deuterium isotopic substitution, the same group provided evidence for a strong isotope effect on the rate, which suggested tunneling as a mechanism for proton transfer.

With picosecond and femtosecond laser techniques in molecular beams, with mass or fluorescence resolution, we made our first real-time study of reaction dynamics in clusters.[13] In an earlier communication,[14] we reported the time-resolved study for the proton-transfer dynamics of 1-NpOH clustered with ammonia, piperidine, and water. The finite-sized clusters of AH·$(NH_3)_n$, AH·$(C_5H_{11}N)_n$, and AH·$(H_2O)_n$ were formed in a molecular beam, and the proton-transfer dynamics of size-specific clusters were studied with the picosecond resolution. Bernstein, Kelley, and their co-workers[15] have investigated the proton-transfer dynamics of AH·$(NH_3)_n$ and studied the effect of isotopic substitution and total energy. Recently, new studies of proton-transfer dynamics in AH·$(NH_3)_n$ have been carried out in this group with subpicosecond time resolution, identifying the elementary process of protonation, deprotonation, and solvent reorganization.[16] Syage et al., in a series of papers,[17] has studied the phenol system and showed the applicability of the approach for the study of solvation effect in real time; with the addition of photoelectron detection, it was possible to directly examine the solvent rearrangement.[18] The present contribution gives a full account of our earlier work and is aimed at understanding the structure and dynamics in these finite-sized solvent cages.

The system under study is generally bimolecular in solutions,

$$A^*H + B_n \rightleftharpoons A^{*-} \cdot \cdot H^+B_n \qquad (3)$$

In the cluster solvent cage,

$$A^*H \cdot \cdot B_n \rightleftharpoons [A^{*-} \cdot \cdot H^+B_n]_u \rightarrow [A^{*-} \cdot \cdot H^+B_n]_e \qquad (4)$$

it defines sharply the processes involved as the system changes from the unequilibrated (u) to equilibrated (e) structures. Because of the weak hydrogen bond, the zero-of-time can be defined, similar to other studies of bimolecular reactions in real time,[19–21] and the diffusion-controlled processes are eliminated. The reversible process in eq 4 depends on a finite number of solvent molecules around the solute, miscible or immiscible,[22] and has analogy in bulk studies of acid reactions. In bulk studies, Huppert et al.[23] and Pines and Fleming[24] have shown the effect of reversibility on the time-dependent form associated with eq 3; the conventional kinetics approach may become inapplicable.

The potential energy surface is normally thought of as a simple double-well, Figure 1. This is because the hydrogen bond is relatively weak and the configurations A*H and H^+B_n are much different. For the ion-pair product state, the shape of the potential energy surface is modified due to Coulombic interaction and the solvent cage effect, as discussed later in the text. If tunneling is the dominant mechanism, then the time for transfer will depend on the nature of the potential (barrier height and width), which is strongly dependent on the intermolecular distance of the solute and the solvent (here, the O–N distance). The rearrangement of solvent molecules is also expected to affect the potential energy surface in both static and dynamical ways.

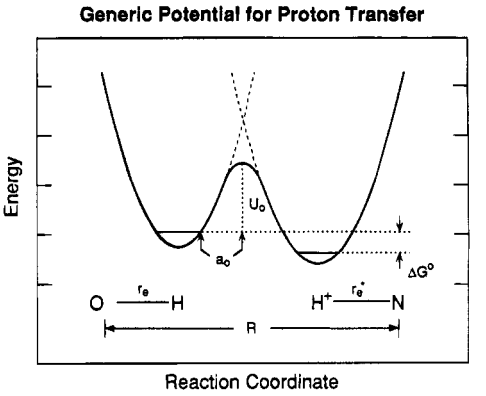

Figure 1. Generic potential of proton-transfer reactions, using two-state model. The barrier height is U_0, and the half-width along the reaction coordinate (q) is a_0. R is defined as the distance between O and N atoms of 1-naphthol and ammonia, respectively. The reaction coordinate for this case is the motion of the proton between two potential minima.

On the time scale of tunneling (a few picoseconds for a barrier of ~0.5-Å width and a height of ~3 kcal/mol), IVR is expected to play a role in the initial transfer and after the transfer. The latter has been shown to be essential in intramolecular hydrogen-atom transfer.[25] In addition, solvent fluctuation and reorganization may or may not influence such redistribution depending on the time scale. Tunneling may not be as simple as the picture in Figure 1 implies. For example, the theoretical study of Ando and Hynes on HCl in water[26] indicates that the final transfer may involve several steps on going from "contact" to "solvent-separated" ion pairs, and this may be similarly the case even in finite-sized systems. These central issues in proton-transfer dynamics are discussed here with focus on measurements of the rates, isotope effect, energy dependence, and the effect of the number and type of solvent molecules. We discuss the energetics, the influence of the cluster structure and size, and the solvent rearrangement on the tunneling dynamics.

The paper is outlined as follows. Section II gives the experimental description, while III summarizes the results. Section IV is the discussion, and in V, the paper is concluded.

II. Experimental Section

Three different experimental setups have been used in these studies. Below we describe each one briefly.

A. Dispersed Fluorescence and Lifetime Measurements. Dispersed fluorescence and lifetime measurements were performed using an experimental setup that has been described in detail in earlier reports from this group.[27,28] Briefly, the setup consisted of a picosecond dye laser combined with a supersonic beam apparatus with time-correlated single-photon-counting equipment. A cavity-dumped dye laser was synchronously pumped by the 514-nm output of a mode-locked argon ion laser (Spectra Physics 2030). The dye solution was prepared by dissolving DCM in a mixture of 30 vol % benzyl alcohol and 70 vol % ethylene glycol (~2.1 mM DCM). For the experiments with bare 1-NpOH, rhodamine 6G in ethylene glycol was used. The visible dye laser output delivered 20–30-nJ pulses of a temporal width of ca. 15 ps as measured by intensity autocorrelation and a spectral width of ca. 5 cm^{-1}. These pulses were frequency-doubled in a $LiIO_3$ crystal and focused into the apparatus.

The free jet was produced via a continuous-flow glass nozzle of ~100-μm diameter. 1-NpOH was stored in a sample holder and heated between 90 and 120 °C. Mixtures of ~3% NH_3 in He or in Ar were passed over the sample before expansion.

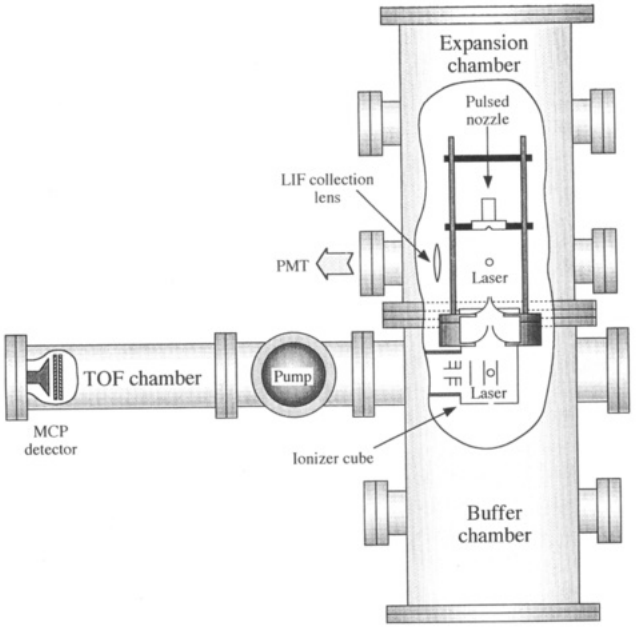

Figure 2. Schematic diagram of the molecular beam system: TOF stands for time-of-flight; PMT for photomultiplier tube; MCP for microchannel plate.

The backing pressures were typically in the range of 30−70 psig. The ensuing free jet and the laser pulses interacted at a sufficiently long distance from the nozzle orifice ($x/d > 30$). Fluorescence was collected in the perpendicular position to the directions of laser pulses and the molecular beam. Fluorescence was detected by a multichannel plate photomultiplier tube (Hamamatsu 2287) after passing through a 0.5-m-long monochromator (Spex Industries). The photomultiplier output was amplified and fed into the photon-counting electronics (ORTEC 457 TAC). The system response was measured to be about 80 ps.

B. Picosecond/Molecular Beam Mass Spectrometry. The experimental apparatus for this setup has been described in detail elsewhere.[14,29] Thus, only the differences involved in performing the experiments reported here [resonant two-photon ionization (R2PI) time-of-flight (TOF) mass detection] to the ones reported before [laser-induced fluorescence (LIF) detection] will be explained in more detail.

The picosecond (pump/probe) laser system consisted of two home-built cavity-dumped dye lasers, synchronously pumped by the second harmonic (532 nm) of a mode-locked Q-switched Nd:YAG laser built from components of a Quantronix Model 416 Nd:YAG laser. The laser dyes used in the experiments reported here were DCM in methanol (pump laser) and DCM in DMSO (probe laser). The FWHM (full width at half-maximum) of the autocorrelation of the visible pump and probe laser pulses was 30−40 ps when fitted to a Gaussian profile. The visible cross-correlation between the pump and the probe laser pulses was about 60 ps when fitted to a Gaussian profile. The spectral widths (Gaussian profile FWHM) were approximately 3 cm^{-1}. Both laser beams were frequency-doubled using either a $LiIO_3$ or a KDP crystal. Typical UV pulse energies were approximately 0.2 mJ. The pump and probe laser pulses were temporarily delayed with respect to each other by passing the pump laser beam through a computer-controlled delay stage. Both lasers were sent via mirrors through a quartz window onto a UV lens ($f = 75$ mm) which was mounted inside the molecular beam apparatus.

The molecular beam apparatus has been described before[14,29] and is schematically shown in Figure 2. The expansion chamber was separated from the buffer chamber by a central flange in which was mounted a skimmer (Beam Dynamics, Model 2, 1.5-mm aperture). For the R2PI experiments, the conical (30°) pulsed nozzle (General Valve, Series 9) was positioned close to the skimmer. The molecular beam entered the ionizer cube mounted inside the buffer chamber through a second skimmer (Beam Dynamics, Model 2, 2-mm aperture) and left it through a 2-mm-diameter hole mounted into the face of the cube opposite the second skimmer. A transition tube connected the ionizer cube and TOF chamber. The center of the ionizer cube coincided with the center line of the TOF drift tube and the molecular beam axis. The laser beams entered through the UV lens mounted in a vertical translation stage which in turn was mounted on the bottom plate of the ionizer cube. Thus, molecular beam, laser beam, and the center line of the TOF drift tube were mutually orthogonal.

The two-stage TOF mass spectrometer allowed for both electron impact ionization, by using an electron gun,[30,31] and photoionization. Its design was based on the Wiley−McLaren scheme.[32] The ions created in the center of the ionizer cube were accelerated via application of a two stage electric field and collimated by an Einzel lens.[33] The ions passed through a 120-cm-long drift tube and were detected by a microchannel plate (Galileo FTD 2003). The ion signal was amplified by a factor of 25 in a 300-MHz preamplifier (Stanford Research Systems, Model SR 240). TOF mass spectra were recorded using a fast waveform analyzer consisting of a 100-MHz transient digitizer (LeCroy 8818A), a memory module (LeCroy MM8103A), and a controller unit (LeCroy 6010 interface controller unit). The analyzer was based in a CAMAC crate (LeCroy 8013A) and triggered by the delay generator (Stanford Research Systems, Model DG535). The data were processed in a microcomputer. The mass resolution achieved with this TOF mass spectrometer was up to $m/\Delta m \approx 200$. The actual transients using only a single mass peak were taken with a boxcar integrator (Princeton Applied Research 162 mainframe and 165 integrator) rather than the transient digitizer.

Backing pressure (4−20 psig), nozzle pulse width, time delay between the opening of the nozzle and the laser interaction, carrier gas composition, and temperature of the 1-naphthol sample (typically 90 °C) were set to maximize the signal of the cluster of interest while minimizing possible interference from other (larger) clusters due to possible fragmentation. The spectroscopic data (excitation wavelength and ionization wavelength) used in these experiments were taken from the work of Leutwyler and co-workers.[8,9] Since the energy necessary to excite the S_1 state of each cluster is higher than 50% of the ionization energy from the S_1 state, one-color R2PI was used as a diagnostic for ensuring optimal ion signals. In the actual two-color pump/probe experiments, care was taken to lower the pump laser power to a minimum in order to prevent ionization by the pump laser alone.

1-NpOH was heated to about 90−120 °C and seeded into a mixture of He and a small percentage (by pressure) of solvent. The nozzle was kept about 10 °C warmer than the sample reservoir in order to prevent clogging. For NH_3, a gas mixture of 0.5−2% NH_3 in He was used. To form clusters with H_2O or piperidine, the partial pressure of the solvent in the expansion was adjusted by controlling the temperature of a wet-line reservoir using a water/ice/sodium chloride bath. The experimental conditions were set to maximize the signal under study while minimizing interference from other clusters. 1-NpOH (Aldrich, 99+%), piperidine (Aldrich, 99%), helium (Big 3 Industries, 99.99%), and ammonia (Matheson, 99.99%) were used without further purification. Under typical experimental

conditions, applying a repetition rate of 100 Hz to the 150-μm-diameter nozzle, the pressure in the expansion chamber was approximately 5×10^{-5} Torr and that in the TOF chamber was about 7×10^{-7} Torr.

For each of the transients measured, a given cluster or group of clusters was excited to the S_1 origin by a UV laser pulse and probed by ionization via a delayed second UV laser pulse. Probe laser wavelengths were chosen to be as red as possible with our laser system while ensuring an acceptable signal level. A typical transient was obtained by averaging the detected signal using the boxcar integrator for each pump−probe time delay. About 50−100 scans were necessary to obtain a transient showing an acceptable signal-to-noise ratio. Small clusters could be excited and detected selectively, so only one mass peak needed to be detected (boxcar method). For larger clusters, a distribution of cluster sizes could be seen in the mass spectrum. In such cases, single cluster transients were obtained either with the boxcar method or alternatively from experiments in which the signal of all clusters was averaged by the transient digitizer at each delay position. In this latter case, individual transients were obtained by processing the data from the averaged mass spectra.

The time constants of the transients were obtained by fitting to single- or double-exponential decays including convolution with the system response function; a Marquardt nonlinear least-squares fitting routine was used.[34] The rising edge of the transients were best fitted by a system response of 60 ps corresponding well to the measured cross-correlation. The zero of time was set to be at the half-maximum of the initial rise of the signal.

C. Femtosecond/Molecular Beam Mass Spectrometry. The setup for the generation of the femtosecond laser pulses used here has been detailed in ref 35. Briefly, a tunable linear-cavity dye laser (Coherent Satori) was synchronously pumped by the frequency-doubled output (532 nm) of a CW mode-locked Nd:YAG laser (Coherent Antares 76S) at a repetition rate of 76 MHz. R610 (or a mixture of KR620 and R640) in ethylene glycol (EG) and DODCI (or Marachite Green) in EG jets were used as the gain medium and saturable absorber, respectively, to generate a laser pulse at 614 (or 640) nm. These laser pulses went through a home-built four-stage pulsed dye amplifier (PDA), pumped by the frequency-doubled output of a 20-Hz Q-switched Nd:YAG laser (Quanta Ray DCR-2). KR620 and R640 in water and SR640 and DCM in methanol were used as gain dyes for amplification. The amplified laser beam was split into two parts by a 30/70 beam splitter. The 30% fraction of the beam was amplified and subsequently passed through a computer-controlled submicrometer resolution delay line, frequency-doubled by a KDP crystal to give the pump laser pulse at 307 (or 320) nm. The other 70% fraction of the beam was focused into a D_2O cell to generate a supercontinuum. From this supercontinuum (white light), a laser beam centered at 680 (or 740) nm was selected by a 10-nm interference filter. The selected laser beam is further amplified by a three-stage home-built PDA using DCM (or LDS698) in methanol to give ~100-μJ pulses. This amplified beam was frequency-doubled using another KDP crystal to generate the probe laser pulse at 340 (or 370) nm. The pulse duration of this system is generally as short as ~100 fs, but for this experiment, we fit the rise to ~600 fs as an operational procedure for handling the decay characteristics at longer times. The spectral widths of pump and probe laser pulses without etalons were measured to be ~7 nm (FWHM). The pump and probe laser pulses were combined using the dichroic beam splitter and focused into the molecular beam chamber.

The molecular beam was prepared by heating a sample of 1-naphthol (Kodak) to 100 ± 20 °C and seeding it in a premixed carrier gas of NH_3 and He (0.5% NH_3 in He) with a backing pressure of 30−40 psig. For the deuterium isotope effect experiment, 1-NpOH in ether was washed with D_2O several times, separated, and collected. To avoid exchange, deuterated ammonia (ND_3) in He was used as the carrier gas. The mixture was then expanded through a pulsed nozzle (0.25-mm diameter) into a vacuum chamber to generate clusters. The resulting cluster expansion passed through a 2-mm skimmer into a second chamber (maintained at $\sim 5 \times 10^{-7}$ Torr), and the molecular beam was crossed with the focused laser beams for time-of-flight (TOF) mass spectrometry.

Using the two-pulse configuration, the mass spectra were collected by a fast digital oscilloscope (LeCroy 9361). The ion signal for a specific mass unit was selected by a gated integrator (SR250) and monitored as a function of the delay time between pump and probe pulses to give the transient for a specific cluster. The transients were averaged over 10 laser shots and 40−60 scans, reaching a signal-to-noise ratio typically of 20 or more. This allowed us to reproduce the nonexponential behavior and to obtain accurate fits. We checked for the linearity of the pump power dependence; the probe power was very weak. We also checked for the effect of the nozzle condition on the observed transient. For example, by varying the delay time between the nozzle opening and the laser, a different ion signal was observed, while the actual form of the biexponential transient was found to be robust (for the 1-NpOH·$(NH_3)_3$ cluster, at two different nozzle-to-laser delay times).

III. Experimental Results

A. Spectroscopy and Preliminaries. Spectroscopic studies were made using mass-resolved R2PI excitation and fluorescence emission.[8,9] For 1-NpOH·$(NH_3)_n$ and 1-NpOH·$(C_5H_{11}N)_n$, a large red shift and a substantial broadening of the excitation spectra as well as a very large red shift and strong broadening of the fluorescence spectra were observed when the cluster size increased. In the ammonia system, $n = 4$ (for the piperidine system $n = 2$) was found to correspond to the onset of spectral changes.[8,9] The observed position and width of the emission were similar to those observed for the 1-naphtholate anion in basic aqueous solutions.[10] For the water clusters, no evidence of such an emission behavior, up to $n = 20$, was found. Even for $n \geq 30$, the position and width did not converge to that of the aqueous 1-naphtholate solutions. Recently, Bernstein and co-workers reported mass-resolved R2PI excitation spectra of 1-NpOH clustered with ammonia and water.[36] Their spectroscopic findings were in agreement with those of Leutwyler and co-workers.

The time-resolved dynamics of proton transfer in the ammonia system[14,15] showed that the critical threshold for the rates was $n = 3$ and that the decay process involves a biexponential behavior, which cannot be deduced from line-width measurements. Because of this discrepancy in n, Bernstein and co-workers reinvestigated the 1-NpOH·$(NH_3)_3$ system and found a red-shifted broad emission which they attributed to proton transfer taking place in at least one geometric isomer of these $n = 3$ clusters.[36] This analysis is consistent with our finding,[14] and Bernstein and co-workers attributed the discrepancy to the severe spectral overlap of the excitation spectra of $n = 2$ and 3 clusters.[36]

The spectroscopic results by Leutwyler's group were very helpful to our work, especially their results on the cluster-size-dependent spectral shifts in the R2PI spectra. These spectral shifts are reproduced in Table 1. By using these results with

TABLE 1: Spectral Shifts of Clusters and Pump/Probe Wavelengths

cluster	spectral shift, cm^{-1}	λ, nm pump	λ, nm probe
1-NpOH	0	317.9	
1-NpOH·$(NH_3)_n$[a]			
$n = 1$	−236	320.4	324.0
$n = 2$ (A)	−276	320.7	324.0
$n = 2$ (B)	−352	321.6	324.0
$n = 3$	−409	322.3	337.5
$n = 4$	−710(50)	323.3	337.5
1-NpOH·$(C_5H_{11}N)_n$[b]			
$n = 1$	−307(25)	320.9	337.5
$n = 2$	≈ −750	320.9	337.5
$n = 3$		320.9	337.5
1-NpOH·$(H_2O)_n$[c]			
$n = 1$	−143(10)	319.4	337.5
$n = 2$	−81	318.7	337.5
$n = 3$	−136	319.1	337.5
$n = 4$	−164	319.6	337.5
$n = 5$	−155/−113[d]	319.9	337.5
$n = 6$	/−107	319.9	337.5
$n = 7$	/−111	319.9	337.5
$n = 8$	−105/−208	319.9	337.5
$n = 9-20$[e]	/−175 to ~ −238	319.9	337.5

[a-c] References 8 and 9. [d] Sharp band position/broad band position. [e] The range of the spectral shifts is shown for $n = 9-20$ clusters.

TOF mass analysis, real-time experiments on individual clusters without significant interference from other clusters were possible in the cases of 1-NpOH·$(NH_3)_n$ ($n = 1-3$), 1-NpOH·$(C_5H_{11}N)_1$, and 1-NpOH·$(H_2O)_n$ ($n = 1-4$). In the other cases, especially for the water clusters, where $n = 8-20$, spectral overlap in the excitation spectra prevented single-cluster experiments and care was taken to adjust the clustering conditions (backing pressure and solvent partial pressure, and the temporal overlap of the gas pulse and the laser pulses) such that the cluster size distribution was peaked near the clusters under investigation. We then used TOF mass selection for the identification of n. The laser wavelengths used for the picosecond pump−probe experiments are listed in Table 1.

B. Fluorescence Lifetime Measurements. By using picosecond time-correlated photon-counting methods, we have measured the emission lifetimes of the bare 1-NpOH and the smaller clusters 1-NpOH·$(NH_3)_n$ ($n = 1, 2$). For $n = 2$, we studied the lifetime of two isomers. For $n \geq 4$, the blue-green emission was observed when the clustering conditions and the excitation wavelength were chosen appropriately. Lifetimes were measured under these conditions. Fluorescence decay curves are shown in Figure 3, and the results of these measurements are given in Table 2. Except for a deviation of the lifetime of the bare 1-NpOH (60 ns) from those of the clusters (38−43 ns), no systematic dependence on the cluster size could be observed. Basically, the solvent shortens the lifetime, evidently because of nonradiative decay.

Leutwyler and co-workers reported emission lifetimes for bare 1-NpOH as well as for the smaller clusters 1-NpOH·$(H_2O)_n$ ($n = 1-5$) from the S_1 origin.[9] They also obtained the decay for the blue-green emission, indicative of the 1-naphtholate anion in experiments where the clustering conditions were set to form large water clusters with $n \leq 50$.[37] The measured lifetimes for $n = 1-5$ varied between 47 and 72 ns, showing no specific monotonic behavior with cluster size. The blue-green emission lifetime averaged over a distribution of larger water clusters was found to be 28 ± 1 ns. For the bare 1-NpOH, they reported a lifetime of 61 ns.

Lakshminarayan and Knee recently reported fluorescence lifetime measurements for the bare 1-NpOH, excited to the S_1 state at different vibrational energies in a molecular beam.[38] These experiments were performed to characterize the dynamics of intramolecular vibrational energy redistribution (IVR) as a function of excess vibrational energy above the S_1 origin. No evidence for rapid IVR was manifested, as initial dephasing was not observed; only restricted IVR among a few levels could be detected, suggesting subnanosecond IVR in the energy range of 0 to 1600 cm^{-1}.

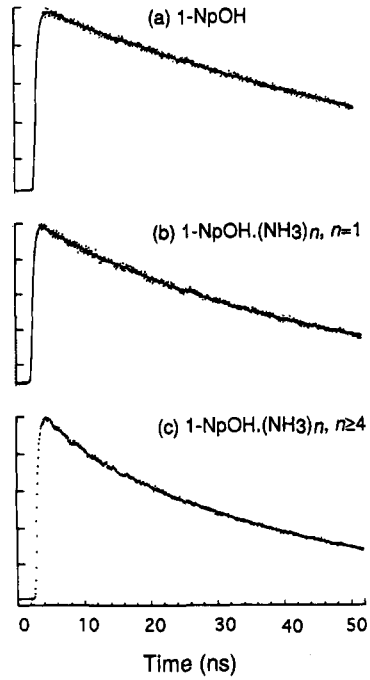

Figure 3. Fluorescence decay curves for (a) bare 1-NpOH, (b) 1-NpOH·$(NH_3)_n$ ($n = 1$), and (c) 1-NpOH·$(NH_3)_n$ ($n \geq 4$) clusters. Excitation and detection wavelengths are listed in Table 2.

TABLE 2: Picosecond Fluorescence Measurements of 1-NpOH·$(NH_3)_n$

cluster size	lifetime, ns	λ, nm excitation	λ, nm detection
bare 1-NpOH	60(2)	318.1	332.8
$n = 1$	38(1)	320.6	335.5
$n = 2$ (A)	43(2)	320.9	335.8
$n = 2$ (B)	39(1)	321.8	336.7
$n \geq 4$	38(1)	322.7	428.0

C. Pump−Probe Transient Measurements. (a) Naphthol−Ammonia ($n = 1-4$) Picosecond Resolution. A typical TOF mass spectrum for 1-NpOH·$(NH_3)_n$ clusters obtained with a laser wavelength of 322 nm is shown in Figure 4. Clusters as large as $n = 30$ were formed in the molecular beam. Figure 5 shows the experimental transients of clusters 1-NpOH·$(NH_3)_n$ ($n = 1-4$) obtained with this picosecond resolution. The pump wavelength was chosen to excite the specific cluster under investigation to minimize interferences from other clusters (Table 1). An exception to this procedure is the system 1-NpOH·$(NH_3)_4$ which has a broad and not well-defined spectral origin. We excited this cluster at 323.8 nm (pump), which differs by 150 cm^{-1} from the reported[8] value of 322.1 nm. However, no significant change in the time-dependent behavior of the transients was observed when changing the excitation wavelength to 322.1 nm. For $n = 2$, two transients are presented, labeled "A" and "B", respectively. These correspond to the two reported isomers for $n = 2$ for which different spectral origins were identified.[8]

For all clusters, 1-NpOH·$(NH_3)_n$ ($n = 1, 2$), the transients obtained show no short-time, *i.e.*, picosecond time scale,

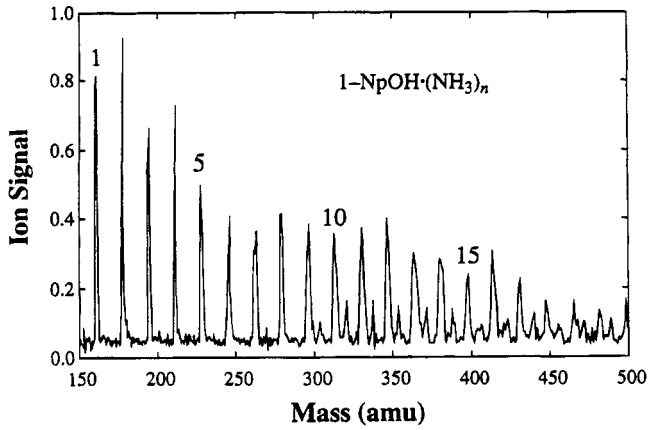

Figure 4. Multiphoton ionization time-of-flight mass spectrum of 1-NpOH·$(NH_3)_n$ showing a typical cluster distribution obtained using the setup described in section II.B.

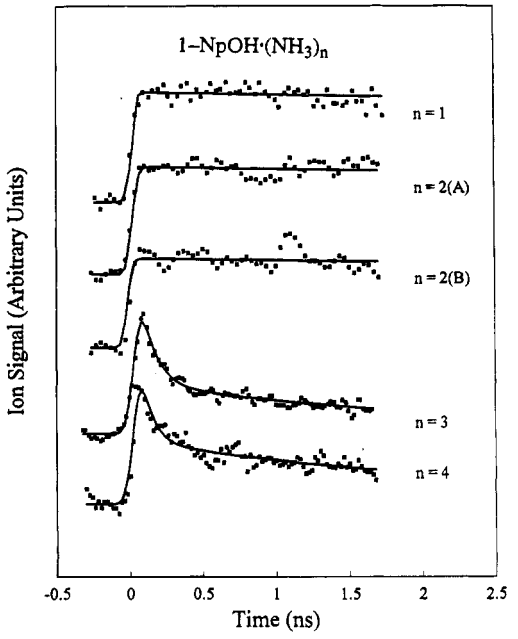

Figure 5. Picosecond (pump−probe) transients recorded for the clusters of 1-NpOH·$(NH_3)_{n=1-4}$. Excitation conditions are listed in Table 1. The solid lines are calculated fits using a double-exponential function (see text).

dynamics. The slight decay observed in the transients at these relatively short times is related to the excited-state lifetimes which are on the order of tens of nanoseconds, Table 2. As the delay line has a usable range of up to 4 ns, these lifetimes could not be reproduced as accurately with the pump−probe apparatus as with the photon-counting results given in section III.B.

For the clusters 1-NpOH·$(NH_3)_n$ (n = 3, 4), the measured transients reveal dynamics on the picosecond time scale. Each of the transients was fitted to a double-exponential decay. The fitted time constant for the fast decay component was 87 ± 30 ps for n = 3 and essentially the same value for n = 4 (in ref 14, τ was 100 ± 30 ps). These measurements were first reported in our earlier communication.[14] The slow decay time constants are estimated to be more than a nanosecond, Figure 5. As discussed below, with subpicosecond resolution, these rates can be obtained more accurately and the form of the transient, short and long decay components, becomes certain in the assignment.

(b) Naphthol−Ammonia (n = 1−6) Subpicosecond Resolution. The proton-transfer dynamics of the ammonia system were studied again with a subpicosecond resolution. In this

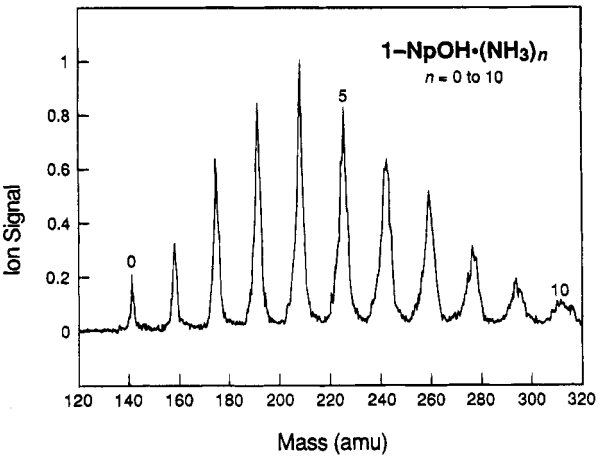

Figure 6. Multiphoton ionization time-of-flight mass spectrum of 1-NpOH·$(NH_3)_n$ showing a typical cluster distribution obtained using the setup described in section II.C.

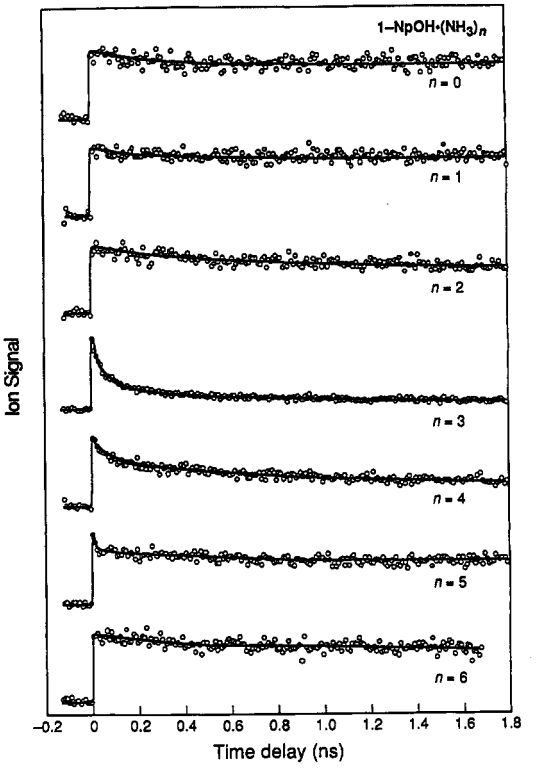

Figure 7. Subpicosecond (pump−probe) transients for 1-NpOH·$(NH_3)_n$, with n varying from 0 to 6. Pump/probe wavelengths are as follows: 320/340 nm for n = 0−4; 320/370 nm for n = 5; and 326/370 nm for n = 6.

apparatus, the cluster distribution obtained is shown in Figure 6. Transients obtained for n = 0 to n = 6 are shown in Figure 7. The transients for n = 0−4 were taken at 320/340 nm (pump/probe), while those for n = 5 and 6 were obtained at 320/370 and 326/370 nm, respectively. With the 320/340-nm arrangement, no time-dependent signal was observed for clusters larger than n = 4, possibly due to ion fragmentation.[39] The transients for clusters of n = 3−5 show an initial fast decay, while the others show relatively slow decay with time constants of tens of nanoseconds, which are comparable to the fluorescence lifetimes of the excited state, Table 2. A very fast initial decay with small amplitude was observed within the first few picoseconds for the n = 5 transient.

The transients for A*H·$(NH_3)_3$ and A*D·$(ND_3)_3$ taken at two different pump energies are shown in Figure 8. These transients show distinct biexponential decays and were fit with a function

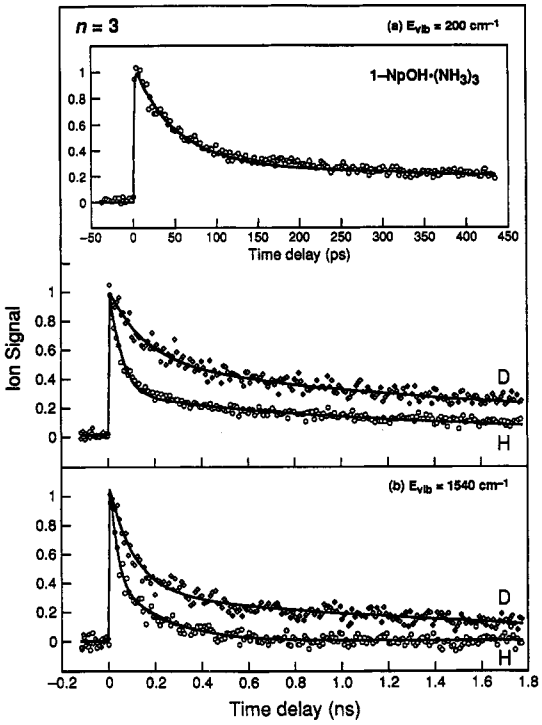

Figure 8. Subpicosecond experimental transients and theoretical fits for 1-NpOH·$(NH_3)_3$ and 1-NpOD·$(ND_3)_3$: (a) pump/probe wavelengths of 320/340 nm and (b) 307/340 nm. Excess vibrational energies are given relative to the origin at 31 050 cm^{-1} for the $n = 3$ cluster.

TABLE 3: Biexponential Fits to Observed Transients of 1-NpOH·$(NH_3)_n$[a]

		H, $n = 3$	D, $n = 3$	H, $n = 4$	D, $n = 4$
320 nm	τ_1	52(4)	150(20)	93(8)	335(200)
	τ_2	1210(60)	>2100	>2700	>8000
	R	2.5	1.0[b]	0.6[b]	0.4[b]
307 nm	τ_1	25(3)	100(10)	70(6)	152(35)
	τ_2	226(20)	1720(150)	727(25)	>5000
	R	2.2	2.1	0.8	0.4[b]

[a] τ_1 and τ_2 are in picoseconds. The values in parentheses are standard deviations. The uncertainty of R, which is defined in the text, is within 20−30%. [b] Less reliable due to large uncertainties of τ_2.

of the form $S(t) = A_0[R \exp(-t/\tau_1) + \exp(-t/\tau_2)]$, which is convoluted with the instrumental response function. The results of the fits for $n = 3$ and 4 clusters are listed in Table 3. The results for the fast decay component are consistent with those obtained with the picosecond resolution of the previous section but provide more accurate time constants. For the long-decay components, the results obtained here are quantitatively quite different from the values given in ref 15. For example, for the $n = 3$ cluster, our fast decay component is 52 ± 4 ps, while the slow component is 1210 ± 60 ps. The results in ref 15 gave 57 ± 15 and 440 ± 125 ps, respectively.

(c) Naphthol−Piperidine ($n = 1-3$) Picosecond Resolution. Figure 9 shows our picosecond real-time results for the 1-NpOH−piperidine clusters. For all the clusters, the same excitation wavelength (320.9 nm) was used in our experiments. This wavelength corresponds to the S_1 origin of the 1-NpOH·$(C_5H_{11}N)_1$ cluster and is within one of the broad bands reported in the R2PI spectrum for the 1-NpOH·$(C_5H_{11}N)_2$ cluster.[8] Again, each transient was recorded individually with the experimental conditions set to maximize the ion signal for the particular cluster under consideration. The probe wavelength was to the red of the excitation wavelength.

Similar to the observations reported for the ammonia clusters, a significant change in the transients can be noticed when

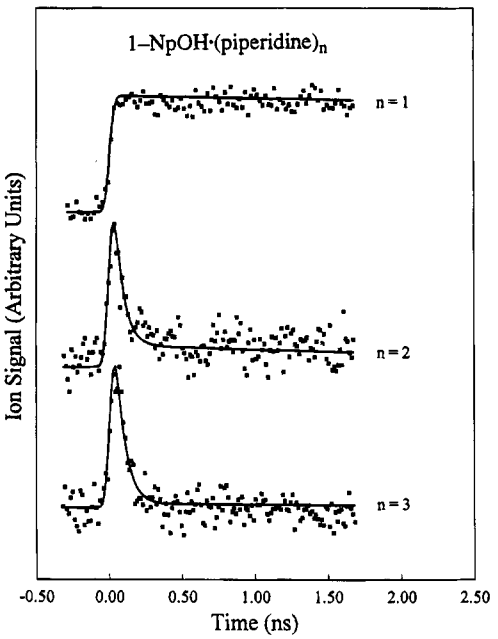

Figure 9. Picosecond (pump−probe) transients obtained for the clusters of 1-NpOH·$(C_5H_{11}N)_{n=1-3}$. Excitation conditions are listed in Table 1. The solid lines are fits using a single-exponential function (see text).

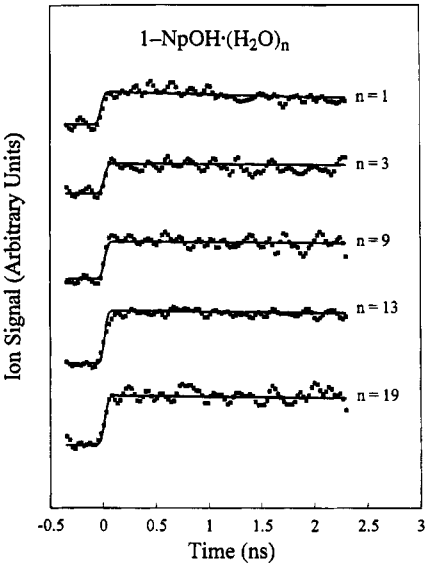

Figure 10. Picosecond (pump−probe) transients obtained for the clusters of 1-NpOH·$(H_2O)_{n=1-19}$. Excitation conditions are listed in Table 1. The solid lines are fits using a single-exponential function (see text).

increasing the cluster size. For the $n = 1$ cluster, a very slight decay on the nanosecond time scale can be seen which is consistent with being due to the excited-state lifetime. Both the $n = 2$ and $n = 3$ clusters reveal picosecond time-scale dynamics. Each of the transients exhibits a characteristic proton-transfer time of ~65 ps. From the transients shown in Figure 9, it can be seen that only the $n = 2$ transients shows a slight leveling off, whereas the $n = 3$ transient reaches the zero background within less than 500 ps.

(d) Naphthol−Water ($n = 1-21$) Picosecond Resolution. In Figure 10, our real-time results of the 1-NpOH·$(H_2O)_n$ ($n = 1-21$) clusters are summarized showing the transients for $n = 1$, 3, 9, 13, and 19. Individual experiments were performed for the water clusters with $n = 1-4$ using the reported cluster origins.[9] The remaining transients were recorded using a transient digitizer with signal-averaging capabilities which

allowed the transients of a number of clusters to be measured in a single experiment. For such experiments, the excitation wavelength was chosen to excite a range of clusters with overlapping R2PI spectra. Two different experiments were performed in order to cover the remaining range of clusters. The excitation wavelength was 320 nm, and the backing pressure was varied from 15 to 30 psig in these two experiments. Thus, the cluster distribution could be shifted to larger n. As can be seen from Figure 10, no dynamics on a short (picosecond) time scale characteristic of proton transfer could be observed.

IV. Discussion

A. Structure of Clusters. The structure of clusters formed in a molecular beam is quite important in determining the energetics and dynamics of the proton-transfer reaction since the solvation energy is closely related to the local structure of the solvent. Felker's group, using rotational coherence spectroscopy, has shown that for the 1:1 complex of 1-NpOH and ammonia the NH_3 is attached to the OH group of 1-NpOH by forming a H bond between (O)H and the N atom.[40] Pratt's group[41] obtained the structure for the 2-NpOH−ammonia complex from the high-resolution spectra; the structure is similar to that of 1-NpOH, with slightly different interatomic distances. Bernstein and co-workers[36] have calculated the most probable structure for the 1:1 complex as the one in which NH_3 resides on the ring of 1-NpOH. For the $n = 2$ cluster, there are two geometrical isomers for which distinct spectral origins were observed. Felker's group found that both NH_3 molecules are attached to the OH group in one geometrical isomer, while for the other isomer the results were suggestive of an NH_3 bound to the ring of 1-NpOH.

For the $AH\cdot(NH_3)_3$ cluster, several geometrical isomers are possible. Felker's group found that at least one of the structural conformers, which corresponds to the relatively sharp spectral origin, has a structure in which all three NH_3 molecules reside on the side of the OH group of a 1-NpOH. Because of the sharpness of the spectra, this structure was assigned to the conformer where no proton transfer took place. Felker's group could not determine the structure of clusters which undergo proton transfer. As discussed below, some ammonia molecules may reside on the ring and affect the energetics involved in the proton-transfer dynamics, thus establishing an interplay between the structure and the dynamics.

Because of the relatively high proton affinity of piperidine, a strong hydrogen bonding is expected between the OH group of 1-NpOH and the N atom of piperidine. Felker's result for piperidine is consistent with this structure.[40] For water clusters, Felker's group found that the water solvent is attached to the OH group of 1-NpOH in both 1:1 and 1:2 (1-NpOH:water) complexes.[40] This is consistent with the calculation by Bernstein and co-workers, who found that the water molecules have a tendency to bind together and reside as a group in the vicinity of the OH group of 1-NpOH.[36] This local structure of the water solvent is not in favor of the solvation of ion-pair states; therefore, it could be one of the factors in preventing the proton-transfer reaction in water clusters.

B. Energetics: The Thermochemical Cycle. We begin by outlining a thermochemical cycle that identifies the energetics of bare 1-NpOH and the stepwise energies of solvation necessary for describing the cluster system. The reaction of interest,

$$AH^*\cdot\cdot\cdot B_n \rightarrow A^{*-}\cdot\cdot\cdot H^+B_n \qquad (5)$$

can be broken down to the following sequence:

$$AH^*\cdot\cdot\cdot B_n \rightarrow AH^*\cdot\cdot\cdot B_{n-1} + B \quad D_n^*$$

$$\vdots$$

$$AH^*\cdot\cdot\cdot B \rightarrow AH^* + B \quad D_1^*$$

$$AH^* \rightarrow AH \quad -h\nu_0^0(AH)$$

$$AH \rightarrow A + H \quad D(A-H)$$

$$H \rightarrow H^+ + e^- \quad E_{IP}(H)$$

$$A + e^- \rightarrow A^- \quad -E_{EA}(A)$$

$$A^- \rightarrow A^{*-} \quad h\nu_0^0(A^-)$$

$$H^+ + B \rightarrow H^+B \quad -D_1^{H^+}$$

$$\vdots$$

$$H^+B_{n-1} + B \rightarrow H^+B_n \quad -D_n^{H^+}$$

$$A^{*-} + H^+B_n \rightarrow A^{*-}\cdot\cdot\cdot H^+B_n \quad V_n^*$$

where AH is shorthand for 1-NpOH and D represents the dissociation energy. The energy terms are known to reasonable accuracy except for the ion-pair bond energy V_n^*. Calculations of Coulombic potentials are presented below. The above description allows us to compare the energetics of gas-phase reactions to cluster reactions and to compare the energetics of proton transfer for different solvents. The enthalpy of the gas-phase deprotonation of AH to form $A^- + H^+$ is given by

$$\Delta H_d = D(A-H) + E_{IP}(H) - E_{EA}(A)$$
$$= 3.60 + 13.60 - 2.51 = 14.69 \text{ eV} \qquad (6)$$

(where the stated values are from refs 42, 43, and 44, respectively). The analogous energy for AH* is given by

$$\Delta H_d^* = \Delta H_d - h\nu_0^0(AH) + h\nu_0^0(A^-)$$
$$= 14.69 - 3.90 + 3.2 = 14.0 \text{ eV} \qquad (7)$$

(where the spectral energies were obtained from spectra in ref 8).[7,45] These very endothermic gas-phase reactions undergo significant stabilization under cluster (or condensed-phase) solvation conditions. The excited-state enthalpy for dissociative proton transfer in clusters of solvent size n (*i.e.*, $AH^*\cdot\cdot\cdot B_n \rightarrow A^{*-} + H^+B_n$) is given by

$$\Delta H_{d,n}^* = \Delta H_d^* + \sum_i^n D_i^* - \sum_i^n D_i^{H^+} \qquad (8)$$

The importance of defining the dissociative proton-transfer enthalpies is that these energies can be determined fairly accurately. A tabulation of stepwise energies and enthalpies for NH_3 solvation is given in Table 4. The proton transfer measured here does not involve a full dissociation; instead, the proton remains bound to the counterion by Coulombic attraction. The enthalpy of proton transfer in clusters is, therefore, given by

$$\Delta H_{PT,n}^* = \Delta H_{d,n}^* - V_n^* - \epsilon_n^* \qquad (9)$$

where we have included an additional solvation energy, ϵ_n^*, that describes further stabilization, due to geometry change or

TABLE 4: Coulombic Potential Parameters for 1-NpOH·(NH_3)[a]

q_O	V_n^*, eV	r_e, Å
−0.2	3.68	1.85
−0.53	3.76	1.8
−0.82	4.43	1.5

[a] Parameters used here are r_{Ph-O} = 2.5 Å, r_{H-N} = 1.04 Å, r_{N-H_3} = 0.52 Å; $q_{ring1} = q_{ring2} = -0.235$; $q_H = 0.54$, $q_N = -1.01$, $q_{H_3} = 1.38$. The repulsive parameters are A = 100 eV and ϱ = 0.32 Å. The potential energy curves for ion-pair states in Figure 11 are calculated using the following parameters: $q_O = -0.53$ and $q_H = +1.0$ ($n = 0$); for n = 2−4, q_H = 0.52, 0.507, 0.49; q_N = −1.06, −1.11, −1.15; q_{H_3} = 1.40, 1.44, 1.47, respectively.

anion solvation that are not explicitly accounted for in the ion-pair bond (along the OH coordinate) energy, V_n^*, or elsewhere in the above thermochemical cycle.

C. Coulombic Interaction and Potential Energy Curves. Here, we consider the form of the potential from an approximate charge distribution in the ion-pair configuration. The ion-pair state representing the proton-transfer product can be described by a Coulombic potential $V(r)$, where r is the O−H internuclear separation. We are interested not only in the well depth V_n, which is needed for the thermochemical expressions, but in the shape of the potential energy curve, which determines the barrier properties and tunneling rates. The potential $V(r)$ is calculated from the sum of the pairwise attraction and repulsion interactions between specific sites i and j (*e.g.*, atoms within a molecule or cluster),

$$V(r) = \sum_{i<j} V_{ij}(r) = \sum_{i<j}\left[\frac{q_i q_j}{r_{ij}} + A\exp\left(-\frac{r_{ij}}{\varrho}\right)\right] \qquad (10)$$

where the q's are charge densities separated by distance r_{ij} and A and ϱ are constants.[46] Such potentials have been introduced by Syage for the phenol system[17,39] and may now define V_n^* (well depth) and the equilibrium distance of the ion-pair state.

Charge densities for $H^+(NH_3)_n$ (up to n = 4) were calculated by Deakyne.[47] The only charge density data we could find for naphtholate was a 1968 molecular orbital calculation[48] and an ESR study;[49] however, they gave very different results for the charge density of the O atom of naphtholate (q_O) of −0.82 and −0.20, respectively, although the ESR work was for the T_1 state. We use charge densities for 1-NpO*$^-$ based on molecular orbital calculations for PhO^- by Taft and co-workers (*i.e.*, q_O = −0.53),[50] which turns out to be close to the average of the two values mentioned above. We computed potential curves for all three cases, and the results together with the potential parameters are given in Table 4, with the following in mind: (1) to simplify the analysis, we have grouped some charges as outlined in Table 4, (2) we adopt the same repulsive parameters used for PhOH·$(NH_3)_n$ (A = 100 eV and ϱ = 0.32 Å), since these values lead to an OH equilibrium bond length of about 1.8 Å for the 1-NpO*$^{-}$·$^{\cdot}$·H^+NH_3 ion-pair state.[40,41,51-53] The calculated ion-pair potentials neglect some potentially important contributions, such as (1) interatomic potential terms (although these should be small relative to V), (2) stabilization of the 1-NpO^- anion by the solvent, and (3) charge redistribution or ion-induced dipole effects that might be transmitted through the O−H bond (*i.e.*, polarizability or dielectric screening).[54] The latter two effects are solvation properties that we relegate to the ϵ_n^* term above in eq 9.

For the bare naphthol ion-pair state, the positive charge resides on the H atom (we assume q_H = 1.0) in close proximity to the negatively charged phenoxy. Hence, at the equilibrium position,

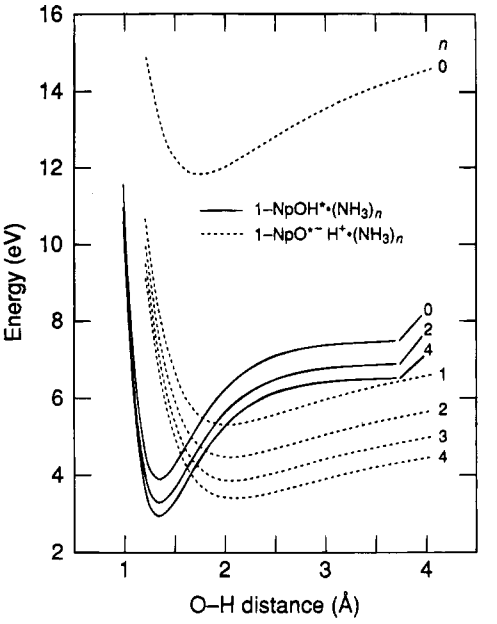

Figure 11. Calculated potential energy curves for 1-NpOH·$(NH_3)_n$ along the O−H coordinate. The ion-pair Coulomb potential parameters are listed in Table 4. The figure gives both the covalent (solid lines) and ionic (dotted lines) potentials and defines the values of V_n^*, the equilibrium distances, and the change of ΔH^* (difference between minima of covalent and ionic potentials).

the Coulombic well depth for bare naphthol is relatively large (V_0^* = 6.1 eV) and the O−H bond length is short (r_e = 1.4 Å). A single NH_3 molecule delocalizes the positive charge, causing the ion-pair bond energy to decrease to V_1^* = 3.8 eV and the bond length to increase to 1.75 Å. Additional solvation further weakens and extends the O−H bond (e.g., V_5^* = 3.1 eV and r_e = 1.9 Å for n = 5).

To complete our picture of the proton-transfer surface crossing, the initially excited S_1 potential curves are fitted to a Morse function of the form

$$V(r) = D\{1 - \exp[-\beta(r - r_e)]\}^2 \qquad (11)$$

The bond energy D is reported in eq 6. We take the equilibrium O−H bond length to be r_e = 0.95 Å.[55] The vibrational amplitude is calculated from the classical turning points of a harmonic oscillator. For an O−H (v = 1) fundamental of frequency 3500 cm^{-1}, one obtains $|r_{max} - r_e| = 0.16$ Å. Fitting eq 11 to these values gives $\beta = 2.25$ $Å^{-1}$. The addition of a single NH_3 molecule does not change the shape of the 1-NpO−H potential curves nearly as much as it lowers the energies relative to uncomplexed naphthol.

Figure 11 and Table 5 illustrate how proton transfer is stabilized in the presence of base molecules. $\Delta H_{PT,n}^*$ changes in value from about 8 eV for n = 0 to about zero for n = 5 (note the difference in energy between minima of the solid and dotted curves, representing the covalent and ionic potentials, respectively). From the observed threshold at n = 3, we assume a value of $\Delta H_{PT,3}^* \leq 0$ compared to a calculated value of 0.78 eV. Our proton solvation/Coulomb model, therefore, accounts for >90% of the observed solvent stabilization energy. Better agreement is expected by including the additional interactions outlined above that were lumped together as solvation energy ϵ_n^*. For example, the Coulomb model favors a solvent geometry in which the second level of NH_3 molecules, which carries 0.07−0.15 units of positive charge for n = 2−4, respectively, establish close proximity to the negative charge density on the O atom or aromatic ring. This would give an additional

TABLE 5: Some Relevant Energies and Enthalpies for 1-NpOH·$(NH_3)_n$ Excited-State Proton Transfer (eV)

i, n	D_i^*	$D_i^{H^+}$	$\Delta H_{d,n}^*$	V_n^*	$\Delta H_{PT,n}^* + \epsilon_n^*$
0			14.00	6.07	7.93
1	0.36[a]	8.84[b]	5.52	3.76	1.76
2	0.25	1.08	4.69	3.50	1.19
3	0.20	0.76	4.13	3.35	0.78
4	0.15	0.60	3.68	3.21	0.47
5	0.15	0.54	3.29	3.10	0.19

[a] D_i^* is obtained from the spectroscopically determined value for PhOH·NH_3 (ref 58), and the remaining values are chosen to converge to the neutral NH_3−NH_3 bond energy of 0.15 eV (ref 62). [b] $D_i^{H^+}$ is the proton affinity of NH_3 (ref 43), and the remaining values are measured stepwise solvation energies (ref 63).

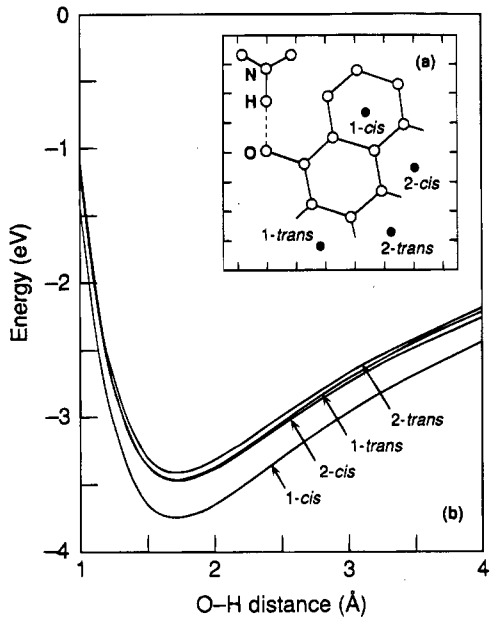

Figure 12. (a) Geometry of NpOH·NH_3 used to calculate Coulomb potentials for different isomers and rotomers of NpOH. The charges q_{ring1} and q_{ring2} are assigned to the center of mass of the aromatic rings marked by a solid circle. The tic marks on the axes represent 1-Å units. (b) Coulombic potentials calculated for the cis and trans rotomers of 1- and 2-NpOH. The dissociative limit is at zero energy.

stabilization of roughly 0.2 eV for charges of say +0.1 and −0.4 separated by 3 Å. It is also possible that NH_3 binds to the ring, which we have not considered in these calculations.

The Coulomb potential is useful for explaining the relative excited-state acidities for the 1-NpOH and 2-NpOH isomers and their cis and trans rotomers. It is apparent from the molecular structure in Figure 12a that the cis rotomer of 1-NpOH permits the closest approach of oppositely charged sites and, therefore, gives the most stable ion-pair state as calculated in Figure 12b. Indeed, the pK_a^* of 0.5 for 1-NpOH is lower than that of 2.8 for 2-NpOH.[7] This corresponds to an energy difference of 0.14 eV, which compares favorably to the calculated Coulomb potential difference (averaging over rotomer energies) of about 0.21 eV. It is interesting that this cis and trans rotomers of 1-NpOH differ in energy by the fairly large value of 0.34 eV. This interpretation may have bearing on the conclusions of Bernstein et al. that only a certain isomer of the 1-NpOH·$(NH_3)_3$ clusters undergoes proton transfer.[36] Note that in the molecular beam the trans rotomer of 1-NpOH is predominantly populated.[36]

We now examine the enthalpy of reaction $\Delta H_{PT,n}^*$ as a function of solvent size using the model for potential energy outlined above. A tabulation of $\Delta H_{PT,n}^* + \epsilon_n^*$ values for NH_3 solvation is given in Table 5. As defined earlier, ϵ_n^* accounts for a certain amount of solvent stabilization energy, which is closely related to the local solvent structure and not accounted for by the simple terms $\Delta H_{PT,n}^*$ and V_n^*. If we assume that the observed threshold at $n = 3$ indicates that $\Delta H_{PT,n}^* < 0$, then one might argue from Table 5 that $\epsilon_3^* > 0.78$ eV. A plot of $\Delta H_{PT,n}^* + \epsilon_n^*$ vs n is presented in Figure 13 for various solvents with 1-NpOH and for NH_3 with phenol. Stepwise solvation energies for $H^+(C_5H_{11}N)_n$ are not known other than for the proton affinity, so only a single point at $n = 1$ and an extrapolation to $n = 2$ are given. Nonetheless, it is evident that piperidine is predicted to give the smallest threshold solvent size for proton transfer for the cases shown, which is in agreement with experiments. The relative ordering of enthalpies of reaction for the other cases in Figure 13 also conforms with the ordering of threshold solvent size observed experimentally. Quantitative predictions of threshold solvent sizes are not obtained by Figure 13 but require a more rigorous theory that avoids the need to invoke the correction factor ϵ_n^*. However, it is encouraging that a smooth and reasonable function for ϵ_n^* can be drawn that crosses with the solvation energy curves (indicating $\Delta H_{PT,n}^* = 0$) at points that are in close agreement with the observed threshold solvent sizes for all cases measured.

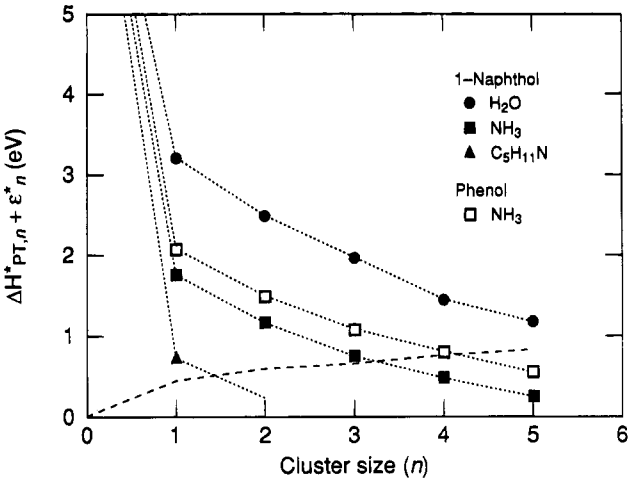

Figure 13. Computed enthalpy of proton transfer as a function of solvent type and size. The dashed line originating from the origin is an estimate of the magnitude of ϵ_n^* and, therefore, represents the line for which $\Delta H_{PT,n}^* = 0$. The proton affinities $D_1^{H^+}$ of piperidine, NH_3, and H_2O are 9.82, 8.84, and 7.36 eV, respectively (ref 43). The curve for piperidine could not be extended because stepwise solvation energies $D_{i>1}^{H^+}$, to our knowledge, are not known.

D. Elementary Steps in Dynamics. Since the observed rates are much slower than those characteristic of coherent wavepacket motion,[13] we shall use rate processes to describe the system outlined in eq 4:

$$A^*H\cdot\cdot B_n \underset{k_{-1}}{\overset{k_1}{\rightleftharpoons}} [A^{*-}\cdot\cdot H^+B_n]_u \xrightarrow{k_2} [A^{*-}\cdot\cdot H^+B_n]_e \quad (12)$$

From the above reaction scheme, it is clear that a biexponential decay would be observed by monitoring the reactant, $A^*H\cdot\cdot B_n$. From the solution of the population equations, it follows that the fast component is determined by $\sim(k_1 + k_{-1})$, while the slow component reflects the effect of the k_2 process. This is true when the ionization cross section of the optically prepared excited states is dramatically decreased to nearly zero when the proton transfers to the solvent in clusters. It is important to realize that eq 12 in the absence of k_{-1} process can also give rise to an apparent biexponential decay if both $A^*H\cdot\cdot B_n$ and

TABLE 6: 1-NpOH·$(NH_3)_n$ (n = 3) System: k_1, k_{-1}, and k_2[a]

E_{vib}, cm^{-1} [b]	time, ps	H, n = 3	D, n = 3
200	$1/k_1$	71(9)	275(40)
(320 nm)	$1/k_{-1}$	200(40)	370[c]
	$1/k_2$	910(60)	>1120
1540	$1/k_1$	35(4)	143(10)
(307 nm)	$1/k_{-1}$	106(30)	357(90)
	$1/k_2$	164(25)	1200(170)

[a] Rate constants are obtained from time constants and ratios listed in Table 3 using the following relations: $1/\tau_1 + 1/\tau_2 = k_1 + k_{-1} + k_2$, $1/(\tau_1\tau_2) = k_1k_2$, and $R = (\alpha + k_1 - k_{-1} - k_2)/(\alpha - k_1 + k_{-1} + k_2)$, where $\alpha = [(k_1 + k_{-1} + k_2)^2 - 4k_1k_2]^{1/2}$. [b] Vibrational energies were calculated relative to the origin at 31 050 cm^{-1} for the n = 3 cluster (see refs 8 and 36), and they represent the average values at the center of our excitation pulses. [c] Less reliable due to uncertainties of values in Table 3.

$[A^{*-}\cdot\cdot H^+B_n]_u$ are assumed to be detectable with different ionization cross sections; a ratio of around 1:0.1−0.3 for $A^*H\cdot\cdot B_n$ and $A^{*-}\cdot\cdot H^+B_n$ can be invoked. In this case, the fast and slow decays represent the proton transfer and solvent reorganization rate, respectively, and the ratio of fast-to-slow decays represents the relative ionization cross sections. The transient for 1-NpOH·$(NH_3)_3$ at 307 nm (where $k_2^{-1} \sim 150$ ps) decays to zero background (Figure 8), suggesting that the final product, $[A^{*-}\cdot\cdot H^+B_n]_e$, is not detectable since one expects for this species a rise with a plateau.

In Table 6, for AH·$(NH_3)_n$, we present the fit parameters to the biexponential form given by eq 12. We note, from Table 6, that the fast rate of transfer is very sensitive to the isotopic substitution and to the total energy, consistent with the trends given in ref 15. With the subpicosecond resolution reported here, we observed no faster decay than the picosecond value given for AH·$(NH_3)_3$. From Table 6, it is apparent that k_1 increases with the total energy and decreases with D substitution. The value of k_{-1} is consistently smaller than that of k_1, and on the time scale of both k_1 and k_{-1}, IVR may play a role. The IVR rate is expected to become faster as the density of states increases in 1-NpOH itself[38] or due to cluster modes.[56] Hence, increasing the vibrational energy, decreasing the vibrational frequencies by H/D isotopic substitution, or increasing the number of degrees of freedom by increasing the number of solvent molecules should increase the rate constant of IVR. The time constants listed in Table 3 show that neither τ_1 nor τ_2 is consistent with the above trend except for vibrational energy. Moreover, some of our measurements were made near the origin where one expects IVR to be on a very long time scale. Accordingly, our scheme in eq 12 does not include an IVR process, although it is part of the description of the solvent reorganization. In the following sections, we discuss the different elementary steps expressed by k_1, k_{-1}, and k_2 and consider the interplay between structures and dynamics.

E. Proton Transfer: Tunneling. The mechanism of proton transfer has been extensively modeled and studied (see, *e.g.*, refs 1−3, 15, and 57). There are mainly three coordinates to be considered: the motion of the proton along the reaction coordinate (q), the vibration of O and N atoms of 1-naphthol and ammonia, respectively, along the intermolecular coordinate (Q), and the motion of solvent molecules along the solvent coordinate (S). The crossing of the S_1 Morse-type potential and the ion-pair Coulomb potential suggests the existence of a barrier to proton transfer, Figure 11. In this case, the potential curve is adiabatic and the crossing is avoided. In clusters, at early times the solvent configuration may be fixed. Accordingly, the proton transfer may be described as tunneling along the q coordinate through the barrier, with the height and width being modulated by the O−N van der Waals stretch motion along the Q coordinate. Experimental evidence for a barrier includes the relatively slow (many picoseconds) rates measured for naphthol, and also for phenol,[17,39] in relatively strong base solvents such as ammonia. Support for a tunneling mechanism is found in results showing reactivity from the vibrationless level of 1-NpOH and a very large deuterium isotope effect in 1-NpOH and in phenol.[15,17,39]

Generally, the semiclassical expression for the tunneling rate constant from bound-to-free (inverted) parabolic potential energy surface is given by[1]

$$k = \nu \exp\left[-\frac{a_0}{\hbar}\pi(2mU_0)^{1/2}\right] \tag{13}$$

where ν is the OH vibrational frequency, m is the effective mass, a_0 is the half-width of the barrier, and U_0 is the barrier height (see Figure 1). Different potentials are used to account for the parameters. For example, Bernstein and co-workers[15] used a model potential energy surface for which the untransferred proton is bound in a well and the transferred proton is a free particle. Syage, on the other hand, used a bound potential instead of a free particle.[17] U_0 and a_0 are strongly modified by the O−N stretching vibrational motion, and these effects can be considered by calculating an expectation value of tunneling rate constant for each quantum state of the O−N stretch.[15]

At the origin, k in eq 13 should be averaged over the zero-point vibrational motion of the O−N stretch;[15] $k(\nu{=}0) = \langle\phi_0|k|\phi_0\rangle$, where ϕ_0 is the harmonic wavefunction for the O−N stretch mode at $\nu = 0$. Then $k(\nu{=}0)$ is given by

$$k(\nu{=}0) = \nu\left(\frac{\alpha}{p}\right)\exp\left\{q\left(\frac{q}{p} + 2a_0\right)\right\}$$

$$\alpha = \frac{4\pi^2\mu\nu_2}{h}$$

$$q = -\frac{\pi^2}{h}(2mU_0)^{1/2}$$

$$p = \alpha - q/2a_0 \tag{14}$$

where ν is the OH vibrational frequency as in eq 13, μ and ν_2 are the reduced mass and frequency of the O−N oscillator, and U_0 and a_0 are the barrier height and width at the equilibrium O−N position as defined above. As the total vibrational energy increases, the probability of being populated in the quantum states of the O−N stretch mode increases and the rate should be averaged over energetically accessible quantum states of the O−N stretch mode. Expressions for tunneling rate constants for vibrationally excited states of the O−N stretch mode are elaborate and are given in ref 15; they have been used to account for the trends of experimental results.

The approximations and limitations of the two-dimensional tunneling model have been discussed before.[15−17] Our intention here is to give an order of magnitude estimate of the rates and to predict their changes, accounting for the following effect and dependencies: deuterium isotope effect, vibrational energy dependence, dependence on barrier height and width, and variations with cluster size. At the origin, the tunneling rate constant can be calculated using eq 14. However, there are several parameters that we must consider. First, ν of ~3500 cm^{-1} in bare 1-NpOH is expected to be lower in clusters with base solvents due to a strong hydrogen bonding. Bernstein and co-workers have estimated ν to be ~3000 cm^{-1}.[15] The frequency of the O−N stretch mode (ν_2) has been estimated to be ~110 cm^{-1} in ref 15, while it has been measured to be ~182

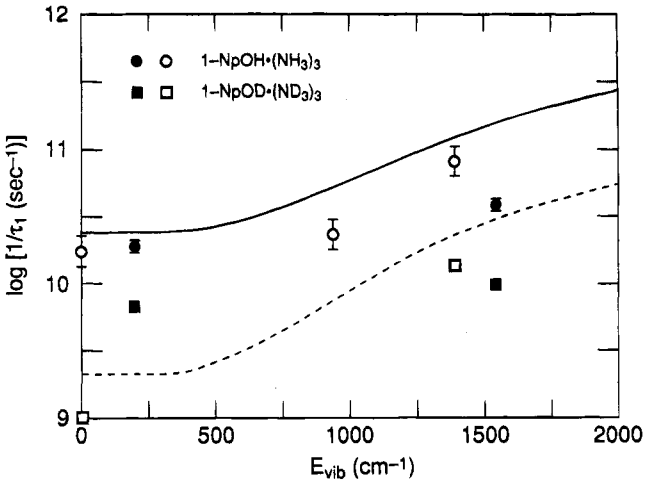

Figure 14. Calculated tunneling rate constants for $AH\cdot(NH_3)_3$ (solid line) and $AD\cdot(ND_3)_3$ (dashed line) as a function of the vibrational energy. The time constants for the fast decay components are plotted from Table 3 (filled circles and squares) and ref 15 (open circles and squares). Parameters for calculation are $\nu(O-H) = 3000\ cm^{-1}$, $\nu(O-D) = 2150\ cm^{-1}$, $\nu_2(O-N) = 110\ cm^{-1}$, $\mu(H) = 38$ amu, $a_0 = 0.2$ Å, and $U_0 = 7500\ cm^{-1}$.

cm^{-1} in the $PhOH\cdot NH_3$ cluster.[58] For the barrier width (a_0), this can be estimated from recent spectroscopic studies.[40,41] According to Pratt's group, the O−N distance in the 2-NpOH•-(NH_3) cluster is ~2.6 and ~2.8 Å in the excited and ground states, respectively.[41] On the other hand, Felker's group determined the O−N distance in 1-$NpOH\cdot(NH_3)_n$ ($n = 1-3$) to be ~3.0 Å.[40] Felker's group reported the average of the ground- and excited-state values. Hence, if it is assumed that the O−N distance in the excited state is ~0.2 Å shorter than that in the ground state, its value will range from 2.8 to 2.9 Å. For the O−N distance of 2.6 and 2.8 Å, a_0 is estimated to be ~0.2 and ~0.3 Å, respectively, by considering the classical turning points of the zero-point energy levels (~0.1 Å) and the O−H and N−H distances (~1.0 Å each). The absolute value of the rate constant for a cluster at the given energy can be fit by varying the barrier parameters. Since the energetics is strongly dependent on the basicity and the number of the solvent (see section IV.B), the shape of the barrier is expected to be unique for the specific cluster under examination. Therefore, it is less meaningful to compare tunneling rate constants for different clusters using the same reaction barrier. Here, we calculate rate constants for the $AH\cdot(NH_3)_3$ and $AD\cdot(ND_3)_3$ clusters as a function of the total vibrational energy. As in ref 15, the vibrational states are assumed to be statistically populated, and the rate constant is averaged over all energetically accessible quantum states of the O−N stretch mode. However, we pointed out in ref 16 that the distribution need not be complete or statistical.

In Figure 14, the calculated tunneling rate constants are compared with the experimental results for $AH\cdot(NH_3)_3$ and $AD\cdot(ND_3)_3$ clusters. The parameters used in the calculation of rate constants are listed in the caption for Figure 14. For comparison with experimental results, the time constants for the fast decay component (τ_1) reported here (Table 3) and in ref 15 are plotted together. The effect of the H/D isotopic substitution near the origin is much smaller than that reported in ref 15. As shown in Figure 14, the proton-transfer rate becomes only 3−4 times slower by the H-to-D substitution, while ref 15 gave ~20 times slower rate for the deuterium cluster. Because of the subpicosecond time resolution, our energy spread is larger than that reported in ref 15 and this may contribute to some difference. However, at an excess vibrational energy of ~1500 cm^{-1}, the ratio of the isotope effect here is similar to that reported in ref 15 (see Figure 14). It is fair to say that calculations based on the tunneling model give reasonable estimates of the rate constants and explain their qualitative trends (see Figure 14).

The free particle tunneling model implies the irreversibility of the proton transfer; the model works only when the product states have a much higher density of states than the reactant states. The experimental results using the reaction scheme in eq 12 suggest that the proton transfer may be reversible before it reaches the final equilibrium. Furthermore, there could be other intermolecular modes that can modify the tunneling barrier. For example, the reaction coordinate O−H−N is not linearly oriented; instead, it has been found that it is tilted,[40,41] which suggests that the bending motion could also modify the barrier parameters. Syage has introduced the activated solvent model to account for the phenol system.[17] The activated solvent model is based on the mechanism that the proton transfer occurs by the nonadiabatic crossing of two adiabatic potential energy surfaces of reactants and products driven by the dynamical solvent effect. This treatment only works in the high-temperature limit and strong-solvation approximation. Most of our experimental results were carried out near the origin; hence, this model has not been tried here.

In the studies of intramolecular proton transfer,[25,59,60] the reaction coordinate is shown to involve low-frequency modes and not the OH stretch vibration. In the intermolecular proton-transfer case, the reaction coordinate is coupled to the solvent coordinate, as one knows that solvent reorganization must take place. Second, from a molecular dynamics point of view, it is not clear that the proton transfer involves only one step. In fact, the study by Ando and Hynes[26] of HCl in water shows a two-step process for the creation of the "contact" and "solvent-separated" ion pairs. Tunneling was shown to be not significant in the first step.[26] It would be interesting to follow the proton-transfer dynamics of the system under study here with molecular dynamics simulations in clusters of different sizes. This will allow us to examine the motion of the individual solvent molecules involved, reaching the dielectric continuum limit in the bulk. This work is currently in progress in collaboration with the Hynes group.

F. Structures and Dynamics: Size Dependence. The structure of the cluster has not been considered explicitly in the energetics discussed in section IV.C. The structure has a significant influence, since V_n (or ϵ_n as defined in section IV.B and C) is closely related to the geometrical structures of the cluster, as discussed earlier (see section IV.C). As mentioned earlier, there could be more than one geometrical isomer for the same-sized cluster. For example, let us consider two geometrical isomers I and II for the $AH\cdot(NH_3)_n$ ($n = 3$) cluster; I has a structure in which all three NH_3 molecules are on the side of the OH group and II has a structure in which two NH_3 molecules are attached to the OH group and one NH_3 resides on the ring. As pointed out by Felker's group,[40] V_n of I is expected to be smaller than that of II since the delocalization of the positive charge in the ion-pair state would be more effective for I than II. In addition, for the geometrical isomer II, Coulombic interaction between ammonia and the naphthol ring would contribute to the increase of V_n. Therefore, from eq 9, structure II would be more favorable for proton transfer than I assuming that the proton affinity remains similar; the stability will depend on the net change in the proton affinity and the ion-pair bond energy upon changing the NH_3 position. This indicates that the energetics and dynamics of proton transfer are critically dependent on the structure. This point is significant even in bulk studies, as discussed in the Introduction.

The size dependence of dynamics is quite dramatic in 1-NpOH·$(NH_3)_n$ clusters (Figure 7). The proton-transfer rate constant for the $n = 4$ cluster is smaller than that of $n = 3$. This trend is consistent with the findings of eq 12. The forward reaction is ~3 times faster than the reverse reaction for $n = 3$. This means that the reaction is exothermic, giving the negative $\Delta G°$. For $n = 4$, the ratio of k_1 and k_{-1} is nearly 1, giving $\Delta G°$ of nearly zero. The sharp initial decay observed for $n = 5$ could be consistent with a continued increase in k_{-1}, giving the small ~20% amplitude. (Note that the excess vibrational energy is larger for the larger clusters and the decay is expected to be faster.)

Based on the energetics without considering the local solvent structure, as shown in Table 5, the experimental results cannot be explained; $n = 4$ is more exothermic than $n = 3$, and we expect a faster rate for $n = 4$. As discussed before, the hydrogen-bonded structure determines the stability of charge separation, and the above trend suggests that the solvent configuration for clusters formed in the molecular beam may become more favorable for reactants, compared to products, as the cluster size increases. But there are other possibilities. For example, for clusters larger than $n = 4$, proton transfer might occur even in the ground state, and the transients for $n = 5$ and 6 clusters in Figure 7 may be due to the significant contribution from ion-pair states in the ground state. The other possibility is the passage through the Marcus inverted region, where the absolute value of $\Delta G°$ exceeds the solvent reorganization energy. In other words, as the number of solvent molecules increases, the free-energy difference exceeds the solvent reorganization, resulting in an increase in the activation energy, hence a smaller rate constant.[17] This description is based on the assumption that strong solvation is the driving force of the proton-transfer reaction.

As discussed in the Experimental Results section, we did not observe proton transfer for clusters with $(H_2O)_n$ of $n \leq 21$. This observation is in line with the results of the spectroscopic work by the groups of Leutwyler[9] and Bernstein.[36] The fact that no proton transfer in the water clusters is detectable is common to both 1-naphthol and phenol.[9,17,36] Although Leutwyler and co-workers observed a moderate red shift of the fluorescence with increasing cluster size, at $n \geq 20$ the emission did not converge, however, to that observed for the naphtholate anion in aqueous solutions. The work of Knochenmuss *et al.*, however, shows that red-shifted naphtholate emission is observed for very large water clusters, 1-naphthol·$(H_2O)_n$ clusters (n up to about 800), that they attribute to proton transfer.[61] The rate constants reported, ranging from 0.5 to 1.5 ns (the rate constant decreases with increasing cluster size), were much slower compared to the time constant of 32 ps measured in liquid water.[10] Knochenmuss *et al.* explained the slow rates measured in clusters as being due to a cold fluxional state of water that impedes proton transfer.[61]

Leutwyler and co-workers interpreted the resistance of water to promote proton transfer, even in relatively large clusters, to water molecules being concentrated around the OH group of the naphthol moiety.[9] The latter interpretation is consistent with the calculations of Bernstein and co-workers,[36] who found that the water molecules tend to concentrate near the OH group of 1-NpOH and prefer to bind to each other rather than to the aromatic system (see section IV.A). Thus, there is incomplete solvation of the naphtholate anion, at least for intermediate-sized clusters, and the proton transfer does not take place. It should be noted that the relevant potential hypersurfaces are multidimensional in nature, and even if there exists a low tunneling barrier along the proton-transfer coordinate, there may be insurmountable barriers along other coordinates which prevent such a favorable situation. These arguments are in line with considerations of the rigidity of the cluster or other geometrical constraints preventing proton transfer.

G. Solvent Reorganization. For the AH·$(NH_3)_n$ clusters, distinct biexponential decays were observed (Figures 7 and 8). According to the model of eq 12, the long-time decay component is related to the irreversible processes of equilibration, as discussed in section IV.D, which could involve fragmentation, IVR, emission, or solvent reorganization. If the fragmentation is one of the processes, then the product would be the H^+·$(NH_3)_n$ complex. But, in contrast to the case of the phenol·$(NH_3)_n$ complex,[17,39] no protonated ammonia complex could be detected in this work. Lifetime of emission has been measured to be tens of nanoseconds (Table 2), and therefore, this process is excluded. Accordingly, the slow decay time in transients is associated with solvent reorganization which includes IVR in the product form. The ion-pair complex is formed on the picosecond time scale, and the solvent rearrangement takes place for further stabilization of the acid–base product state. The reorganization requires the dissociation and formation of hydrogen bonds as well as the "rotation" of solvent molecules. In the clusters at low temperatures, the time scale for solvation is therefore expected to be slower compared to that in bulk media. Recent time-resolved photoelectron spectroscopic studies showed that the time constant for solvent reorganization in phenol–ammonia clusters is around 300 ps.[18] Syage found that for the phenol system, the Franck–Condon distribution for ionization is shifted by solvent reorganization to increase the total ion signal. But for the naphthol system, even when it is assumed that the ion-pair state before the solvent rearrangement, $[A^{*-}\cdot \cdot H^+B_n]_u$, is detectable, the solvent reorganization seems to decrease the ionization cross section. Actually, the ion signal went down to zero background in transients for AH·$(NH_3)_3$ taken at 307 nm (pump), Figure 8.

The dependence of τ_2 or $1/k_2$ on vibrational energy, cluster size, and H/D isotope substitution is quite noticeable (see Tables 3 and 6). The time constant decreases as the vibrational energy increases. For the $n = 3$ cluster, $1/k_2 \sim 910$ ps at the vibrational energy (E_{vib}) ~ 200 cm^{-1} decreases to $1/k_2 \sim 164$ ps at $E_{vib} \sim$ 1540 cm^{-1}. This dependence is more dramatic than that for proton transfer. As the total vibrational energy increases, the intermolecular vibrational motions are increasingly excited, thus facilitating the solvent motion, hence, an increase in the rates. The deuterium effect on k_2 is also large. For example, $1/k_2 \sim$ 1.2 ns for AD·$(ND_3)_3$ at $E_{vib} \sim$ 1540 cm^{-1} is ~7 times larger than $1/k_2 \sim$ 164 ps for AH·$(NH_3)_3$ at the same E_{vib}. This suggests the involvement of the intermolecular modes in solvent motion associated with solvent reorganization.

The dependence of τ_2 on the cluster size is shown in Table 3. The time constant $\tau_2 \sim 1.2$ ns for $n = 3$ cluster at $E_{vib} \sim$ 200 cm^{-1} increases to $\tau_2 > 2.7$ ns for $n = 4$ at an even higher vibrational energy (see the spectral shifts in Table 1). As the cluster size gets larger, the number of intermolecular modes associated with solvent motions increases. The solvent reorganization along a certain coordinate is accordingly expected to be slower as the probability of populating this coordinate decreases with the number of modes increasing. The solvation energies associated with solvent motions are not accurately known, and, therefore, one cannot rule out the possibility of the existence of structural isomers which undergo different (or no) proton-transfer dynamics. As discussed before, the reaction coordinate must involve the solvent motions, and the local structure of the solvent is therefore critical.

Finally, we should mention that the solvation effect on excited dipoles is expected and has been examined by, e.g., the change of fluorescence with time.[64] Therefore, the excitation of $AH{\cdot}B_n$ could lead to reorganization even in the absence of proton transfer. However, as shown in Figure 8, the proton transfer occurs on a much shorter time scale than the reorganization, and in the "absence" of proton transfer in higher n clusters (Figure 7), we do not observe the characteristic decay of the reorganization observed when, e.g., $n = 3$ and proton transfer is present.

V. Conclusions

In this paper, we reported real-time picosecond and subpicosecond studies of solvation involving proton-transfer reactions in clusters. The solute/solvent systems are 1-naphthol−(ammonia)$_n$ ($n = 1-6$), 1-naphthol−(piperidine)$_n$ ($n = 1-3$), and 1-naphthol−(water)$_n$ ($n = 1-21$), all prepared in a molecular beam. The occurrence of proton transfer on the picosecond time scale was observed for the ammonia clusters at a critical number of solvent molecules where $n = 3$, while for piperidine $n = 2$. The water clusters show no sign of short time scale (picosecond) dynamics for $n = 1-21$, indicating no evidence of proton transfer in these solvent clusters. To understand the nature of the transfer and the role of structural changes, we made the following studies: (1) accurate measurements of the transient decay and its form (biexponential, etc.); (2) the isotope effect; (3) the vibrational energy dependencies; (4) the effect of the number and type of solvent molecules. From these results, we describe a simple model which takes into account deprotonation by tunneling process, protonation, and solvent reorganization.

The distinct cluster size thresholds for proton transfer and the variation among different solvents was explained in the model by considering the thermodynamics of solvation and the Coulombic potential energies for the ion-pair state. Though we use a rather simple approach, important insights were gained. For example, the model is able to explain why 1-naphthol is a stronger acid than 2-naphthol and why a certain isomer of 1-naphthol$\cdot(NH_3)_n$ can be reactive. The barrier to proton transfer is due to a crossing of a *covalent* reactant state and a *Coulombic* ion-pair state. The characteristic proton-transfer times of 50−100 ps were well reproduced in the model by the simple tunneling between two states. The role of tunneling was examined and the origin of the barrier was tested by comparing calculated rates to the measured rates reported here and to other observations made elsewhere.

The importance of the local structure of solvent molecules in determining the proton-transfer dynamics was discussed. It is suggested that the overall dynamics of the transfer is governed by the interplay between the energetics and the solvent effective dielectric screening which determines the strength of the Coulombic interactions of the ion pairs. By considering the rates of deprotonation and protonation and the cluster size dependence, we conclude that the change in free energy with the structural changes shifts the equilibrium toward the acid as the cluster size increases. The critical value found for the number of solvent molecules ($n = 3$ for NH_3; $n = 2$ for piperidine; $n > 21$ for H_2O) for proton transfer elucidates the key role of the local structure on proton transfer, a central point to the argument made in bulk studies by Eigen, Robinson, and others. We are currently involved in further studies of the molecular dynamics under these stepwise solvation conditions in these and other acid−base reactions.

Acknowledgment. We are very happy to contribute this paper on the special occasion of Mostafa's 60th birthday (in the transition state to Georgia Tech). His scientific contributions and services are greatly appreciated, and we wish him many more years of productive and happy life—keep up the smile! We thank Professors P. M. Felker, E. R. Bernstein, and M. Okumura for helpful discussions. We also acknowledge the help of Drs. P. Cong, M. Gutmann, and J.-K. Wang during the different stages of this research. Finally, we thank the two referees for the thorough reading of the manuscript. This work is supported by a grant from the National Science Foundation.

Note Added in Proof. Very recent publications have reported on studies of the naphthol−water system in clusters (fluorescence) and ice crystals. The findings are relevant to the discussion in this paper. See: Oi, P.; *et al. Chem. Phys. Lett.* **1994**, *230*, 322; Knochenmuss, R. D.; Smith, D. E. *J. Chem. Phys.* **1994**, *101*, 7327. Also, see the article on complexes of 2-naphthol with cyclodextrins for structural modeling: Park, H.-R.; *et al. J. Phys. Chem.* **1994**, *98*, 6158.

References and Notes

(1) (a) Bell, R. P. *The Proton in Chemistry*; Chapman & Hall: London, 1973. (b) Bell, R. P. *The Tunnel Effect in Chemistry*; Chapman & Hall: London, 1980.

(2) Special issues of *Chem. Phys.*: (a) Barbara, P. F., Trommsdorff, H. P., Eds. *Chem. Phys.* **1989**, *136*, 153. (b) Benderskii, V. A., Goldanskii, V. I., Jortner, J., Eds. *Chem. Phys.* **1993**, *170*, 265. (c) Agmon, N., Levine, R. D., Eds. *Chem. Phys.* **1994**, *183*, 167.

(3) (a) Kosower, E. M.; Huppert, D. *Annu. Rev. Phys. Chem.* **1986**, *37*, 127. (b) Barbara, P. F.; Walker, G. C.; Smith, T. P. *Science* **1992**, *256*, 975. (c) Arnaut, L. G.; Formosinho, S. J. *J. Photochem. Photobiol. A: Chem.* **1993**, *75*, 1, 21. (d) Kearley, G. J.; Fillaux, F.; Baron, M. H.; Bernnington, S.; Tomkinson, J. *Science* **1994**, *264*, 1285.

(4) Weber, K. *Z. Phys. Chem.* **1931**, *B15*, 18.

(5) (a) Förster, T. *Naturwiss* **1949**, *36*, 186. (b) Förster, T. *Z. Elektrochem.* **1950**, *54*, 531.

(6) Weller, A. *Z. Elektrochem.* **1952**, *56*, 662.

(7) (a) Harris, C. M.; Selinger, B. K. *J. Phys. Chem.* **1980**, *82*, 1366. (b) Ireland, J. F.; Wyatt, P. A. H. *Adv. Phys. Org. Chem.* **1976**, *12*, 131.

(8) (a) Cheshnovsky, O.; Leutwyler, S. *Chem. Phys. Lett.* **1985**, *121*, 1. (b) Cheshnovsky, O.; Leutwyler, S. *J. Chem. Phys.* **1988**, *88*, 4127.

(9) (a) Knochenmuss, R.; Cheshnovsky, O.; Leutwyler, S. *Chem. Phys. Lett.* **1988**, *144*, 317. (b) Knochenmuss, R.; Leutwyler, S. *J. Chem. Phys.* **1989**, *91*, 1268.

(10) (a) Webb, S. P.; Yeh, S. W.; Philips, L. A.; Tolbert, M. A.; Clark, J. H. *J. Am. Chem. Soc.* **1984**, *106*, 7286. (b) Lee, J.; Robinson, G. W.; Webb, S. P.; Phillips, L. A.; Clark, J. H. *J. Am. Chem. Soc.* **1986**, *108*, 6538. (c) Webb, S. P.; Philips, L. A.; Yeh, S. W.; Tolbert, L. M.; Clark, J. H. *J. Phys. Chem.* **1986**, *90*, 5154. (d) Lee, J.; Griffin, R. D.; Robinson, G. W. *J. Chem. Phys.* **1985**, *82*, 4920.

(11) Eigen, M.; DeMaeyer, L. In *The Structure of Electrolytic Solutions*; Hamer, W. J., Eds.; Wiley: New York, 1959 and references therein.

(12) (a) Brucker, G. A.; Kelley, D. F. *J. Chem. Phys.* **1989**, *90*, 5243. (b) Brucker, G. A.; Kelley, D. F. *Chem. Phys.* **1989**, *136*, 213. (c) Swinney, T. C.; Kelley, D. F. *J. Phys. Chem.* **1991**, *95*, 2430.

(13) Zewail, A. H. *Femtochemistry—Ultrafast Dynamics of the Chemical Bond*; World Scientific: NJ, 1994 and references therein.

(14) Breen, J. J.; Peng, L. W.; Willberg, D. M.; Heikal, A.; Cong, P.; Zewail, A. H. *J. Chem. Phys.* **1990**, *92*, 805.

(15) Hineman, M. F.; Brucker, G. A.; Kelley, D. F.; Bernstein, E. R. *J. Chem. Phys.* **1992**, *97*, 3341.

(16) Kim, S. K.; Wang, J.-K.; Zewail, A. H. *Chem. Phys. Lett.* **1994**, *228*, 369.

(17) (a) Steadman, J.; Syage, J. A. *J. Chem. Phys.* **1990**, *92*, 4630. (b) Syage, J. A.; Steadman, J. *J. Chem. Phys.* **1991**, *95*, 2497. (c) Syage, J. A. *Faraday Discuss. Chem. Soc.*, in press. (d) Syage, J. A. *J. Phys. Chem.* **1993**, *97*, 12523. For reviews see: Syage, J. A. In *Femtosecond Chemistry*; Manz, J., Wöste, L., Eds.; VCH: New York, 1994.

(18) (a) Syage, J. A. *Chem. Phys. Lett.* **1993**, *202*, 227. (b) Syage, J. A. *Z. Phys. D* **1994**, *30*, 1.

(19) Scherer, N. F.; Khundkar, L. R.; Bernstein, R. B.; Zewail, A. H. *J. Chem. Phys.* **1987**, *87*, 1451.

(20) Ionov, S. I.; Brucker, G. A.; Jaques, C.; Valachovic, L.; Wittig, C. *J. Chem. Phys.* **1993**, *99*, 6553.

(21) Wright, S. A.; Tuchler, M. F.; McDonald, J. D. *Chem. Phys. Lett.* **1994**, *226*, 570.

(22) Pribble, R. N.; Zwier, T. S. *Science* **1994**, *265*, 75.

(23) Huppert, D.; Pines, E.; Agmon, N. *J. Opt. Soc. Am.* **1990**, *B7*, 1545.

(24) Pines, E.; Fleming, G. R. *Chem. Phys.* **1994**, *183*, 393.

(25) Herek, J. L.; Pedersen, S.; Bañares, L.; Zewail, A. H. *J. Chem. Phys.* **1992**, *97*, 9046.
(26) Ando, K.; Hynes, J. T. In *Structure, Energetics, and Reactivity in Aqueous Solution*; Cramel, C. J., Truhlar, D. G., Eds.; in press.
(27) Lambert, W. R.; Felker, P. M.; Zewail, A. H. *J. Chem. Phys.* **1984**, *81*, 2217.
(28) (a) Felker, P. M.; Zewail, A. H. *J. Chem. Phys.* **1985**, *82*, 2975. (b) Baskin, J. S.; Zewail, A. H. *J. Phys. Chem.* **1989**, *93*, 5701.
(29) (a) Breen, J. J.; Willberg, D. M.; Gutmann, M.; Zewail, A. H. *J. Chem. Phys.* **1990**, *93*, 9180. (b) Willberg, D. M.; Gutmann, M.; Breen, J. J.; Zewail, A. H. *J. Chem. Phys.* **1992**, *96*, 198. (c) Gutmann, M.; Willberg, D. M.; Zewail, A. H. *J. Chem. Phys.* **1992**, *97*, 8037, 8048.
(30) Pollard, J. E.; Cohen, R. B. *Rev. Sci. Instrum.* **1987**, *58*, 32.
(31) Khundkar, L. R. Ph.D. Thesis, California Institute of Technology, 1989.
(32) Wiley, W. C.; McLaren, I. H. *Rev. Sci. Instrum.* **1955**, *26*, 1150.
(33) See: Carrasquillo, E.; Zwier, T. S.; Levy, D. H. *J. Chem. Phys.* **1985**, *83*, 4990.
(34) Press, W. H.; Flannery, B. P.; Teukolsky, S. A.; Vetterling, W. T. *Numerical Recipes in C*; Cambridge University: Cambridge, 1988.
(35) Sims, I. R.; Gruebele, M.; Potter, E. D.; Zewail, A. H. *J. Chem. Phys.* **1992**, *97*, 4127.
(36) Kim, S. K.; Li, S.; Bernstein, E. R. *J. Chem. Phys.* **1991**, *95*, 3119.
(37) Kappes, M.; Leutwyler, S. In *Atomic and Molecular Beam Methods*; Scoles, G., Bassi, D., Buck, U., Laine, D., Eds.; Oxford University: New York, 1988; Vol. 1.
(38) Lakshminarayan, C.; Knee, J. L. *J. Phys. Chem.* **1990**, *94*, 2637.
(39) (a) Steadman, J.; Syage, J. A. *J. Am. Chem. Soc.* **1991**, *113*, 6768. (b) Steadman, J.; Fournier, E. W.; Syage, J. A. *Appl. Opt.* **1990**, *29*, 4962. (c) Steadman, J.; Syage, J. A. *J. Phys. Chem.* **1991**, *95*, 10326.
(40) Connell, L. L. Ph.D. Thesis, University of California, Los Angeles, 1992.
(41) Plusquellic, D. F.; Tan, X.-Q.; Pratt, D. W. *J. Chem. Phys.* **1992**, *96*, 8026.
(42) (a) Moylan, C. R.; Brauman, J. I. *Annu. Rev. Phys. Chem.* **1983**, *34*, 187. (b) Comita, P. B.; Brauman, J. I. *Science* **1985**, *227*, 863.
(43) (a) McMillen, D. F.; Golden, D. M. *Annu. Rev. Phys. Chem.* **1982**, *33*, 493 and references therein. (b) Lias, S. G.; Liebman, J. F.; Levin, R. D. *J. Phys. Chem. Ref. Data* **1984**, *13*, 695.
(44) Lias, S. G.; Bartmess, J. E.; Liebman, J. F.; Holmes, J. L.; Levin, R. D.; Mallard, W. G. *J. Phys. Chem. Ref. Data* **1988**, *17*, 1.
(45) The difference in spectral energies of 0.7 eV is close to the value of 0.55 eV obtained from the well-known thermochemical cycle, eqs 1 and 2.
(46) Martin, T. P. *J. Chem. Phys.* **1980**, *72*, 3506.
(47) Deakyne, C. A. *J. Phys. Chem.* **1986**, *90*, 6625.
(48) Nishimoto, K.; Forster, L. S. *J. Phys. Chem.* **1968**, *72*, 914.
(49) Yagi, M.; Muramoto, A.; Higuchi, J. *J. Phys. Chem.* **1990**, *94*, 1309.
(50) Pross, A.; Radom, L.; Taft, R. W. *J. Org. Chem.* **1980**, *45*, 818.
(51) This is consistent with the heteroatom O- -H- -N distance of about 2.8 Å determined spectroscopically (refs 40, 41, and 52) and the known N−H bond distance of 1.0 Å (ref 53).
(52) Matsuyama, A.; Imamura, A. *Bull. Chem. Soc. Jpn.* **1972**, *45*, 2196.
(53) (a) Price, J. M.; Crofton, M. W.; Lee, Y. T. *J. Chem. Phys.* **1989**, *91*, 2749. (b) Price, J. M.; Crofton, M. W.; Lee, Y. T. *J. Phys. Chem.* **1991**, *95*, 2182.
(54) Arnett, E. M. In *Proton-Transfer Reactions*; Caldin, E., Gold, V., Eds.; Wiley: New York, 1975; p 79.
(55) Schultz, M.; Burgi, T.; Leutwyler, S.; Fischer, T. *J. Chem. Phys.* **1993**, *98*, 3763.
(56) Lienau, C.; Heikal, A.; Zewail, A. H. *Chem. Phys.* **1993**, *175*, 171.
(57) (a) Borgis, D.; Lee, S.; Hynes, J. T. *Chem. Phys. Lett.* **1989**, *162*, 19. (b) Borgis, D.; Hynes, J. T. *J. Chem. Phys.* **1991**, *94*, 3619. (c) Borgis, D.; Hynes, J. T. *Chem. Phys.* **1993**, *170*, 315. (d) Cukier, R. I.; Morillo, M. *J. Chem. Phys.* **1989**, *91*, 857.
(58) Mikami, N.; Okabe, A.; Suzuki, I. *J. Phys. Chem.* **1988**, *92*, 1858.
(59) Elsässer, T. In *Femtosecond Chemistry*; Manz, J., Wöste, L., Eds.; VCH: New York, 1994.
(60) Arthen-Engeland, Th.; Bultmann, T.; Ernsting, N. P.; Rodriguez, M. A.; Thiel, W. *Chem. Phys.* **1992**, *163*, 43.
(61) Knochenmuss, R.; Holtom, G. R.; Ray, D. *Chem. Phys. Lett.* **1993**, *215*, 188.
(62) (a) Ceyer, S. T.; Tiedemann, P. W.; Mahan, B. H.; Lee, Y. T. *J. Chem. Phys.* **1979**, *70*, 14. (b) Greer, J. c.; Ahlrichs, R.; Hertel, I. V. *Chem. Phys.* **1989**, *133*, 191.
(63) (a) Kebarle, P. *Annu. Rev. Phys. Chem.* **1977**, *28*, 445. (b) Grimsrud, E. P.; Kebarle, P. *J. Am. Chem. Soc.* **1973**, *95*, 7939.
(64) See: *Activated Barrier Crossing*; Fleming, G. R., Hänggi, P., Eds.; World Scientific: Singapore, 1993.

JP942299B